O-Methylation of the glycopeptidolipid acyl chain defines surface hydrophobicity of *Mycobacterium abscessus* and macrophage invasion

Wassim Daher[1,4,&], Louis-David Leclercq[2,&], Albertus Viljoen[1,3], Jona Karam[1], Yves F. Dufrêne[3], Yann Guérardel[2], and Laurent Kremer[1,4,#]

[1]Centre National de la Recherche Scientifique UMR 9004, Institut de Recherche en Infectiologie de Montpellier (IRIM), Université de Montpellier, 1919 route de Mende, 34293, Montpellier, France.

[2]Univ. Lille, CNRS, UMR 8576 - UGSF - Unité de Glycobiologie Structurale et Fonctionnelle, F-59000 Lille, France.

[3]Louvain Institute of Biomolecular Science and Technology, Université Catholique de Louvain, Croix du Sud, 4-5, bte L7.07.07., B-1348, Louvain-la-Neuve, Belgium.

[4]INSERM, IRIM, 34293 Montpellier, France.

[#]To whom correspondence should be addressed: Tel: (+33) 4 34 35 94 47;
E-mail: laurent.kremer@irim.cnrs.fr

[&]These authors contributed equally to that work.

Mycobacterium abscessus, an emerging pathogen responsible for severe lung infections in cystic fibrosis patients, displays either smooth (S) or rough (R) morphotypes. The S-to-R transition is associated with reduced levels of glycopeptidolipid (GPL) production and is correlated with increased pathogenicity in animal and human hosts. While the structure of GPL is well established, its biosynthetic pathway is incomplete. In addition, the biological functions of the distinct structural parts of this complex lipid remain elusive. Herein, the *fmt* gene encoding a putative *O*-methyltransferase was deleted in the *M. abscessus* S variant. Subsequent biochemical and structural analyses demonstrated that methoxylation of the fatty acyl chain of GPL was abrogated in the *Δfmt* mutant and this defect was rescued upon complementation with a functional *fmt* gene. In contrast, introduction of *fmt* derivatives mutated at residues essential for methyltransferase activity failed to restore GPL defects, indicating that *fmt* encodes an *O*-methyltransferase. Unexpectedly, phenotypic analyses showed that *Δfmt* was more hydrophilic than its parental progenitor, as demonstrated by hexadecane-aqueous buffer partitioning and atomic force microscopy experiments with hydrophobic probes. Importantly, the invasion rate of THP-1 macrophages by *Δfmt* was reduced by 50% when compared to the wild-type strain. Together, these results indicate that Fmt *O*-methylates the lipid moiety of GPL and plays a substantial role in conditioning the surface hydrophobicity of *M. abscessus* as well as in the early steps of interaction between the bacilli and macrophages.

Keywords: *Mycobacterium abscessus*, glycopeptidolipid, *O*-methyltransferase, hydrophobicity, phagocytosis, atomic force microscopy.

Infections caused by non-tuberculous mycobacteria (NTM) are increasing globally and are usually difficult to treat due to their inherent resistance to many common antibiotics [1]. Among NTM, *Mycobacterium abscessus* is a fast-growing species and an emerging human pathogen that causes nosocomial skin and soft tissue infections [2] but also pulmonary infections, especially in patients with cystic fibrosis (CF) and other lung disorders [3,4]. Like other NTM, *M. abscessus* exhibits either smooth (S) or rough (R) colony morphotypes, which are associated with distinguishable *in vitro* and *in vivo* phenotypes. This colony-based distinction relies on the production of high (in S) or low (in R) levels of surface-associated glycopeptidolipids (GPL) [5–7]. Comparative genomic and transcriptomic studies have been conducted to better understand the molecular mechanisms responsible for the S-to-R transition in *M. abscessus*, revealing multiple insertions or deletions occurring in the R variants, mainly in the *mps1, mps2, gap,* and *mmpL4b* genes that are involved either in the synthesis or transport of GPLs [8]. Epidemiological surveys showcased the prominence of the *M. abscessus* R strain in patients with severe pulmonary infections [9,10] and with chronic colonization of the airways in CF patients [10], underlining that the distinction between S and R morphotypes is of paramount importance and clinically relevant. Indeed, numerous studies have emphasized that the presence or loss of GPL conditions important physiological and physiopathological aspects of infection, among which changes in sliding motility, biofilm formation and susceptibility to antibiotics have been reported [5,7,11–13]. Other properties related to the GPL content have been disclosed, such as bacterial surface hydrophobicity [14,15], aggregation leading to cord formation [5,13,14,16], interaction with and intracellular trafficking in macrophages [17,18] and induction of a pro-inflammatory response [19], all influencing the clinical outcome of the disease. This has also been raised by recent studies using various cellular and animal models, confirming the increased pathogenesis of the R over the S form [13,16,20,21]. In particular, the zebrafish model of infection has been proposed as a relevant and genetically tractable host-pathogen conjugate for dissecting *M. abscessus* interactions with host cells [22], which clearly showed that the S-to-R transition is associated with exacerbation of the bacterial burden, the formation of massive serpentine cords, abscess formation and increased larval killing [16]. The mycobacterial cell envelope comprises, from the inside to the outside, a plasma membrane surrounded by the peptidoglycan layer, covalently connected to an arabinogalactan layer, which itself is attached to the outermost membrane bilayer, designated the mycomembrane [23,24]. The inner leaflet of this outer membrane is predominantly composed of mycolic acids while the outer leaflet contains a mixture of free lipids, such as triacylglycerol (TAG), diacylglycerol (DAG) and a series of complex lipids, including trehalose mono- and di-mycolate as well as GPL. From a structural point of view, GPL are composed of a lipopeptide ornamented with a flexible arrangement of glycosylation that is built from *O*-methylated and *O*-acetylated deoxy hexoses [18,25,26] **(Figure 1A)**. The peptidic core consists of a D-phenylalanine-D-*allo*threonine-D-alanine tripeptide linked to an L-alaninol. This D-Phe-D-*allo*Thr-D-Ala-L-alaninol sequence is assembled by two non-ribosomal peptide synthetases, Mps1 and Mps2, and acylated with a 3-hydroxy/methoxy C_{24}-C_{33} fatty acid by an unidentified acyltransferase [26–28]. The lipopeptide core is

glycosylated with the *allo*-Thr linked to a 6-deoxy-α-L-talose (6-dTal), while the alaninol is linked to an α-L-rhamnose (Rha), producing the less-polar diglycosylated GPL species. In addition to the diglycosylated GPL that contain a 3,4-di-*O*-acetylated 6-dTal and a 3,4-di-*O*-methylated or 2,3,4-tri-*O*-methylated Rha [18,26,29], *M. smegmatis* and *M. abscessus* also produce more polar GPL by the addition of a 2,3,4-tri-hydroxylated Rha to the alaninol-linked 3,4-di-*O*-methyl Rha [26,30]. Although being structurally identical, triglycosylated GPL are more abundant in *M. abscessus* than in *M. smegmatis* [26]. GPL are heterogenous in structure and vary according to the fatty acyl chain length and the degree of hydroxylation or *O*-methylation of the glycosidic moieties through the action of various *O*-glycosyltransferases, *O*-methyltransferases and *O*-acetyltransferases [31] **(Figure 1A)**. Interestingly, a recent study revealed unexpected structural features of the GPL content in *M. abscessus* grown on CF sputum or synthetic CF medium, consisting of an increase in the amount of triglycosylated forms and possible replacement of the classical carboxy terminal alaninol by other branched-chain aminol alcohol, valinol or leucinol [32]. Despite the relevance of GPL in NTM of clinical significance, the GPL biosynthetic pathway, which has been well delineated in *M. smegmatis* and *M. avium* [25,33-36], is only partly described in *M. abscessus*. The individual role of several genes compulsory for GPL production, particularly modifications of the lipid part of GPL, remains to be experimentally investigated. In addition, whether changes in the acyl chain influences the surface properties of *M. abscessus* and eventually its early interaction with host cells remains undetermined. In this study, we questioned as to whether *fmt*, a gene located within the GPL biosynthetic locus of *M. abscessus* **(Figure 1B)** participates in GPL biogenesis.

Construction of a genetically-deficient *fmt* mutant was used to demonstrate that *fmt* encodes an *O*-methyltransferase. Importantly, deletion of *fmt* abrogated *O*-methylation of the fatty acyl chain of GPL, which strongly impacted the bacterial surface properties and phagocytosis of *M. abscessus* by human macrophages. Overall, this study advances our understanding of the genetic requirements for the biosynthesis and biological functions of the high-GPL producing variant of this understudied human pathogen.

4
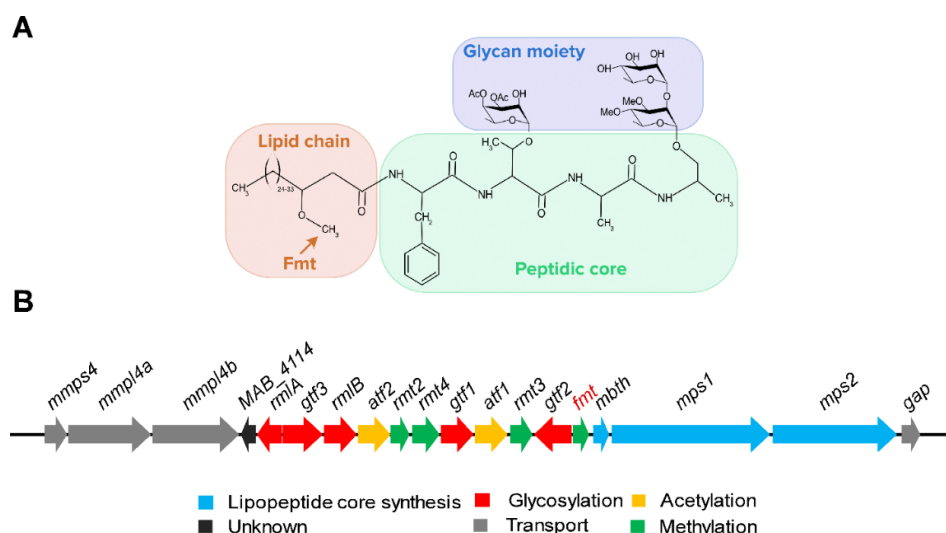
Figure 1. The biosynthetic locus and structure of *M. abscessus* GPL. (A) The lipid, peptidic and glycan moieties of GPL are indicated by different colors. The schema illustrates the triglycosylated form of GPL (GPL-3) consisting of a D-Phe-D-*allo*Thr-D-Ala-D-alaninol peptidic core (green) of which the D-*allo*Thr is glycosylated with a 3, 4 di-*O*-acetyl 6-deoxy-L-talose residue and the alaninol is diglycosylated with rhamnose and 3,4-di-*O*-methylated rhamnose residues. The three monosaccharides are presented in the blue area. The orange arrow shows the methyl group, presumably transferred by the fatty acid *O*-methyltransferase enzyme (Fmt) onto position 3 in the lipid chain (orange area). **(B)** The GPL locus encodes multiple components required for biogenesis, modification and transport of GPL. *fmt* is indicated in orange.

RESULTS

Loss of *fmt* affects neither growth nor colony morphology of *M. abscessus in vitro.* To get insights into the function of the Fmt protein, conventional gene inactivation was performed in the high-GPL producing *M. abscessus* S variant using an unmarked deletion system [37]. The strategy involves double homologous recombination leading to the removal of the *fmt* open reading frame from the GPL locus **(Figure 2A)** using the pUX1-*katG* suicide construct, which carries a kanamycin resistance (*kan^R*) cassette, a tdTomato red fluorescence marker and a *katG* cassette that confers sensitivity to isoniazid, an antitubercular drug to which *M. abscessus* is naturally resistant [37]. Two DNA sequences flanking *fmt* were cloned adjacently to each other into pUX1-*katG* effectively leading to an *fmt*-deleted allele in the resulting pUX1-*katG-fmt* vector. After transformation, clones that integrated pUX1-*katG-fmt* into their chromosome *via* a first homologous recombination were isolated by their resistance to kanamycin and their red fluorescence. A subsequent second homologous recombination step resulting in the loss of pUX1-*katG-fmt* allowed isolation of potential *Δfmt* clones by their resistance to isoniazid, loss of red fluorescence and kanamycin sensitivity. PCR and sequencing screens on genomic DNA using primers listed in **Table S1** confirmed the genotype of a *Δfmt* mutant **(Figure 2B).** To confirm that *fmt* alone was responsible for any phenotypic defects observed in *Δfmt*, the mutant was complemented by site-specific integration at the L5 mycobacteriophage chromosomal attachment site [38] of a C-terminally HA-tagged *fmt* copy under control of its endogenous promoter **(Figure 2C)**. Western blotting was carried out by loading an equal amount of total protein extracts (confirmed by the KasA protein internal loading control). A band with the approximate molecular weight expected for the Fmt-HA protein was detected in the complemented strain, designated *ΔfmtC*.

Since it is well established that the absence or the presence of GPL conditions the morphotype of *M. abscessus* colonies on agar medium, we next assessed whether disruption of *fmt* influences the morphology of the strain. Serial dilutions of cultures were plated on Middlebrook 7H10 or on LB agar and single colonies were observed after 4-5 days of incubation. No visual differences in the morphology were noticed between the WT (S morphotype), *Δfmt* and *ΔfmtC* colonies, regardless of the medium used; and these strains did not show the typical serpentine cords typifying the R variant **(Figure 2D)**. Moreover, *Δfmt* failed to aggregate in liquid culture but produced homogenous suspensions similar to *M. abscessus* S cultures **(Figure 2E)**. The *in vitro* growth curves in 7H9 broth at 37°C were also similar for the S, *Δfmt* and *ΔfmtC* strains, indicating that

deletion of *fmt* does not impact on the replication rate of *M. abscessus* in planktonic culture **(Figure 2F)**. In the same line, like the S progenitor, *Δfmt* produced fragile pellicles at the air-liquid interface **(Figure 2G)**.
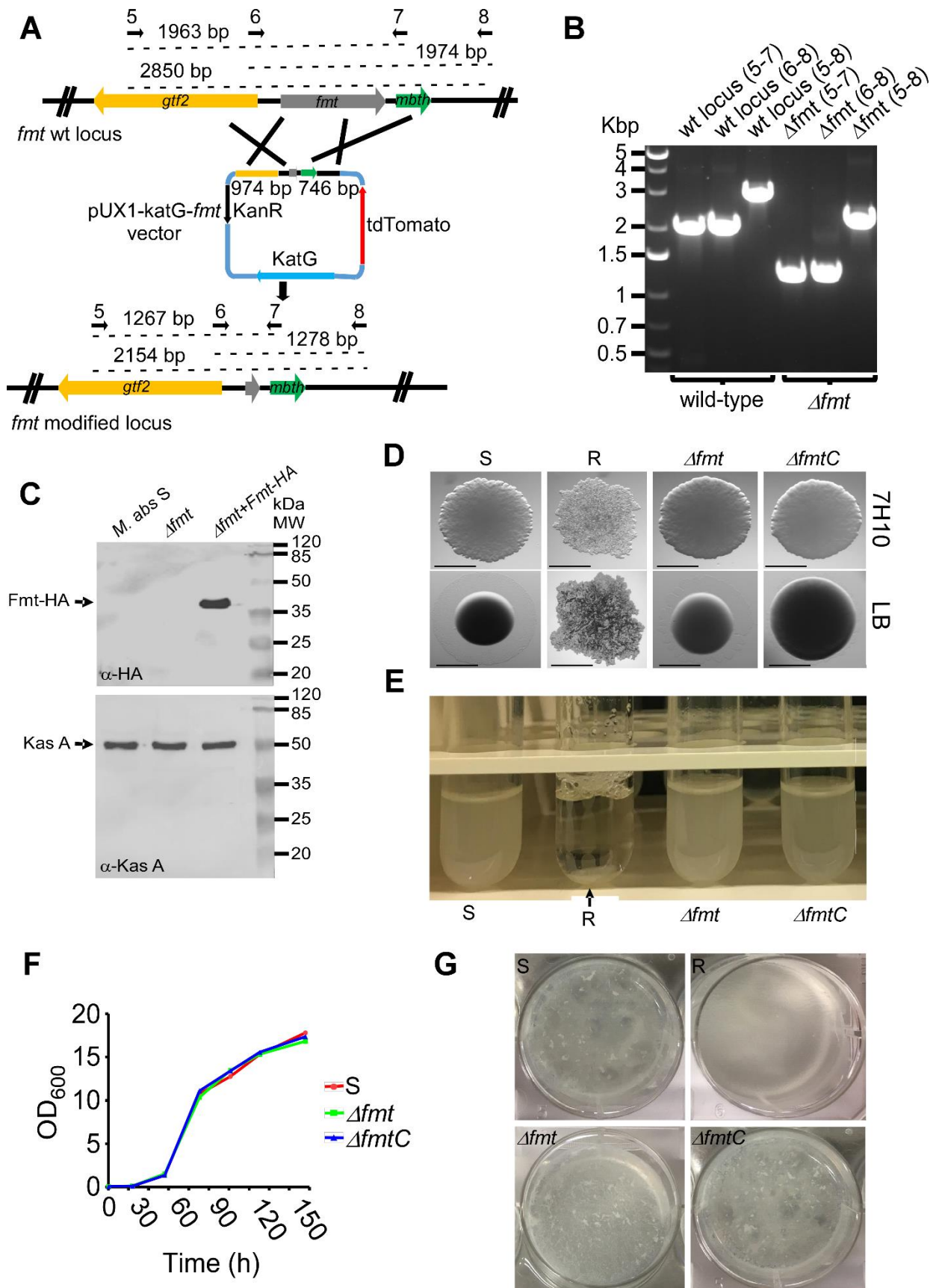
Figure 2. Generation of an unmarked *fmt* deletion mutant in *M. abscessus*. (A) The *fmt* gene is neighbored by the genes *gtf2* and *mbth*. To generate *Δfmt*, two sequences of 974 bp and 746 bp located upstream and downstream of *fmt* were cloned into pUX1-*katG*. The resulting suicide plasmid (lacking motifs for episomal replication or mobile elements promoting chromosomal integration) was used to transform *M. abscessus*, in which it could only propagate *via* homologous recombination between the cloned sequences and their chromosomal homologous sequences. A first recombination event was favored in the absence of antibiotic and clones in which a cross-over occurred were selected in the presence of kanamycin. A single red fluorescent tdTomato-expressing clone was selected and subjected to the second round of recombination. Clones in which a second recombination event occurred were selected on isoniazid and screened for double cross-over phenotypes, *i.e.* loss of red fluorescence, sensitivity to kanamycin and resistance to isoniazid. Dotted lines represent the size (indicated above each line) of the expected PCR products in *M. abscessus* WT and *Δfmt*. Black arrows represent the primers used for PCR analysis. **(B)** PCR analysis demonstrating deletion of *fmt* in the mutant strain. Genomic DNA from WT bacteria was used to amplify the intact *fmt* locus. Amplicons were subjected to sequencing to confirm deletion of *fmt*. **(C)** Western blot analysis of the *ΔfmtC* strain expressing the Fmt protein in fusion with an HA tag under the control of the native *fmt* promoter. KasA was included as a loading control. **(D)** Colony morphology of the S, R, *Δfmt* and *ΔfmtC* strains either on 7H10^OADC or LB plates. No difference in colony morphology between the progenitor S and *Δfmt* strains was found, regardless of the media used. Experiments were carried out twice. **(E)** Like the parental S strain, but unlike the R variant, *Δfmt* does not sediment rapidly in liquid culture. The arrow indicates the sedimented bacterial aggregates. **(F)** Growth curve analysis of parental S, *Δfmt* and *ΔfmtC* strains in 7H9 medium at 37°C. Data is representative of three independent experiments. **(G)** Pellicle-forming capabilities of *M. abscessus* S, R, *Δfmt* and *ΔfmtC* strains. Experiments were carried out twice.

Disruption of *fmt* alters the overall GPL profile in *M. abscessus*. GPL are a heterogenous family of polar glycolipids whose structures have been well established in several NTM, including *M. abscessus* [18,25,26]. Individual GPL comprises three structural parts, a Phe-*allo*Thr-Ala-alaninol peptidic core, a lipid chain and a glycan moiety. In *M. abscessus*, a C_{24}-C_{33} methoxylated 3-hydroxy fatty-acyl chain esterifies the amino group of the Phe, while the *allo*Thr and alaninol are substituted by a 6-dTal and by one or two methylated Rha residues, respectively **(Figure 1A)**. The presence of one or two Rha residues differentiates diglycosylated (GPL-2) from triglycosylated (GPL-3) GPL species. The impact of *fmt* deletion on the overall GPL profile was first analyzed by lipid extraction and separation by thin-layer chromatography (TLC). As anticipated, GPL production was abrogated in the *M. abscessus* R morphotype whereas the S variant produced large amounts of highly heterogenous di- and triglycosylated GPL **(Figure 3A)** [26]. Major differences were noticed in the migration profile between the S variant and *Δfmt*, presumably resulting from small chemical changes in individual molecules. Two rounds of migration showed that the modified GPL pattern in *Δfmt* comprises GPL species that were either produced in lower amounts or accumulating. Importantly, the wild-type (WT) GPL profile was restored in *ΔfmtC*, indicating that the altered GPL profile cannot be attributed to a polar effect caused by the gene deletion in *Δfmt*.

To qualitatively analyze GPL-2 or GPL-3 from WT S and *Δfmt* strains, an in-depth analysis was carried out. Partial purification of the GPL-2 and GPL-3 fractions was accomplished by liquid flash-chromatography on a silica gel column and monitored by TLC analysis **(Figure 3B)**. Starting from the lower part of the TLC to the solvent front, two intense and sharp bands, tentatively identified as trehalose-containing lipids with unsaturated C_{16} and C_{18} fatty acids (data not shown) were observed along with multiple bands with higher

7

R$_f$ values, corresponding to GPL-3 and GPL-2, based on their respective mobilities. These fractions were next subjected to thorough structural analyses.
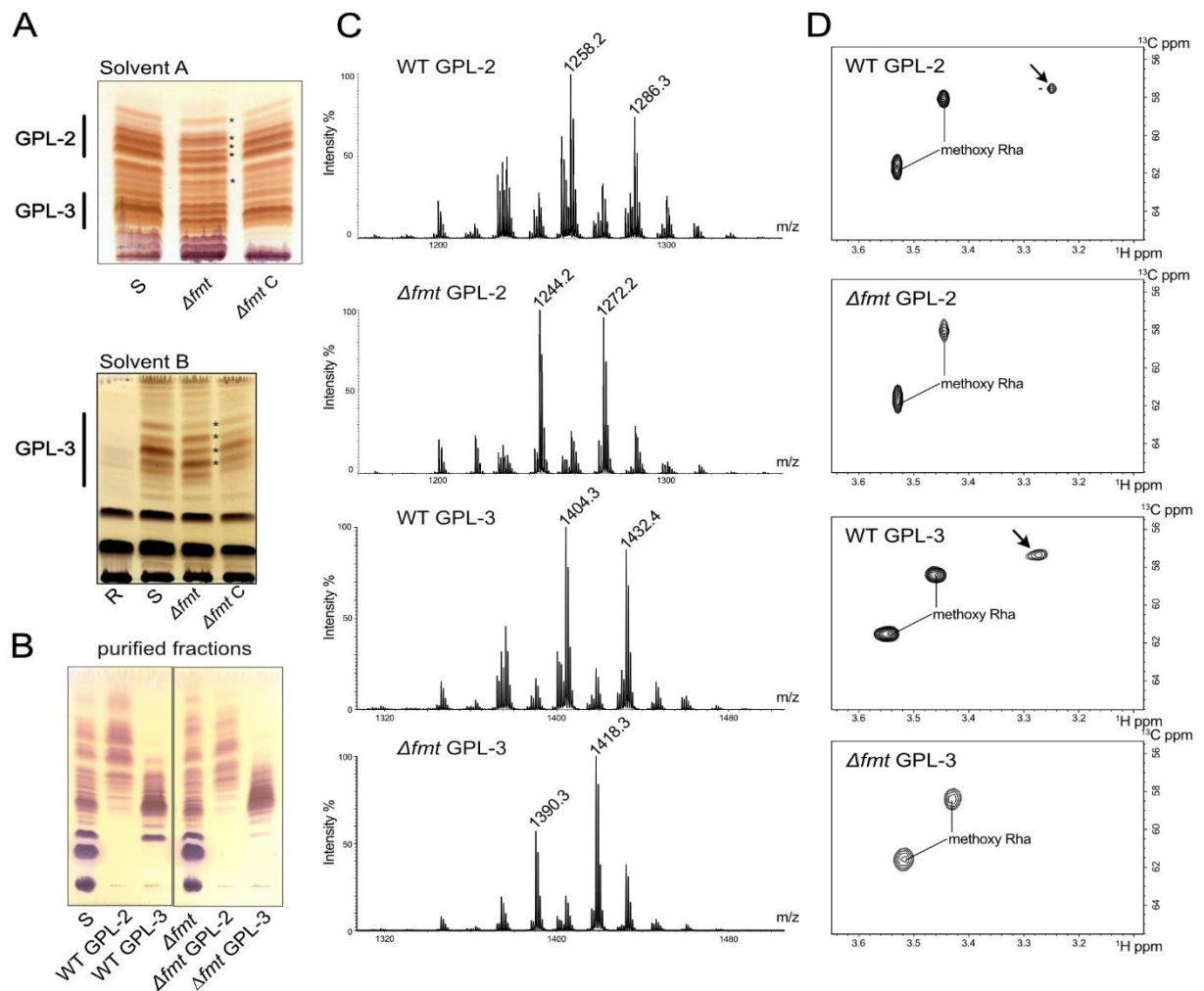

Figure 3. Loss of fatty acid methylation on GPL from _Δfmt_. (A) TLC analysis of the crude lipid fractions of the parental, mutant and complemented strains. GPL-2 and GPL-3 were separated using either solvent A (CHCl$_3$/MeOH 95:5, v/v; upper panel) or solvent B (CHCl$_3$/MeOH 9:1, v/v; lower panel) and revealed with orcinol staining after two rounds of migration. GPL are expressed at similar levels in the parental (S), _Δfmt_ and _ΔfmtC_ strains but are absent in the R variant. Mobility of diglycosylated and triglycosylated GPL species differ in _Δfmt_ as compared to the WT and _ΔfmtC_ strains (upper panel). **(B)** Diglycosylated fractions (GPL-2) and triglycosylated fractions (GPL-3) were separated by flash chromatography and visualized on TLC. **(C)** MS spectra of GPL-2 and GPL-3. The two upper panels correspond to GPL-2 fractions while the two lower panels correspond to GPL-3 fractions. A decrease of 14 m.u. is observed between WT and _Δfmt_ GPL fractions. **(D)** ^{1}H/^{13}C HSQC spectra of purified GPL fractions show methoxy functions substituting either the Rha or the lipid moiety. The methoxy group on the lipid moiety is exclusively found on WT GPL-2 and GPL-3 at δ 3.27/57.4 ppm, as indicated by an arrow.

The glycan moiety of GPL is not altered in the _Δfmt_ strain. The monosaccharide composition determined by GC/MS of WT GPL-2 showed the presence of 3,4 di-_O_-methyl Rha and 6-dTal in an approximate 1:1 ratio. Very similar results were obtained with the _Δfmt_ GPL-2 fraction **(Figure S1)**. Both WT GPL-3 and _Δfmt_ GPL-3 showed the presence of 3,4 di-_O_-methyl Rha, 6-dTal and Rha in approximate 1:1:1 ratio **(Figure S2)**. In

8

addition, 3-*O*-methyl Rha was observed in much lower quantities on all chromatograms, suggesting the presence of minor glycoforms. These results not only confirm that GPL-3 lipids correspond to extended GPL-2 lipids with an additional Rha residue but also imply that loss of *fmt* does not influence the monosaccharide composition of GPL. Mass spectrometry analysis of GPL-2 and GPL-3 from WT and *Δfmt* showed complex patterns of signals dominated by two major signals with 28 m.u. increments, tentatively attributed to two CH_2 groups **(Figure 3C)**. The 146 Da increment between WT GPL-2 and WT GPL-3 major signals at *m/z* 1258/1286 and at *m/z* 1404/1432 was tentatively attributed to a deoxyhexose, confirming that WT GPL-3 corresponds to WT GPL-2 with an extra Rha residue, in agreement with GC/MS analysis and previous reports [26,31]. The fine sequence of individual WT GPL was further delineated by MS^2 fragmentation of the intense ions at *m/z* 1258 **(Figure 4A)** and 1404 **(Figure S3A)**. The presence of terminal Me_2Rha and Ac_2dTal residues in WT GPL-2 was established owing to primary fragment ions at *m/z* 1084 and 1010, respectively, and confirmed by secondary ion products at *m/z* 836 and 454 (**Figure 4A**). In contrast, WT GPL-3 was characterized by a terminal Rha and Ac_2dTal residues owing to primary fragment ions at *m/z* 1258 and 1156 and to a number of secondary ions products (**Figure S3A**), confirming that WT GPL-3 was further elongated by a single Rha residue on the Me_2Rha as compared to WT GPL-2. Similar results were obtained on 28 m.u. higher parent ions for GPL-2 and GPL-3 at *m/z* 1286 and 1432 corresponding to a longer lipid chain (data not shown). The presence of the two acetyl groups on dTal residues to form Ac_2dTal was confirmed by MS and MS/MS analyses of mild alkali treated GPL that led to an 84 m.u. decrease for the molecular ion as well as for all fragments containing the dTal residue. This is exemplified by the MS analysis of saponified WT GPL-3 that shows two signals at *m/z* 1319 and 1347 **(Figure S4A)** as compared to ions at *m/z* 1404 and 1432 for the non-treated fraction **(Figure 3C)** and confirmed by the corresponding MS/MS fragmentation patterns **(Figure S4B)**.

As for WT, the MS spectra from *Δfmt* GPL-2 and *Δfmt* GPL-3 showed complex patterns dominated by major ions with 146 m.u. increments at *m/z* 1244/1272 and *m/z* 1390/1418, respectively, exhibiting a 14 m.u. decrease compared to WT GPL-2 and WT GPL-3 **(Figure 3C)**, tentatively assigned to the loss of a methyl group on *Δfmt* GPL. MS^2 fragmentation patterns of the major GPL species **(Figure 4B and Figure S3B)** and of their alkali-treated equivalents (data not shown) established that the glycan moieties of *Δfmt* GPL-2 and *Δfmt* GPL-3 were identical to those of WT GPL-2 and WT GPL-3. These results clearly indicate that deletion of *fmt* does not alter the glycan moiety of GPL.
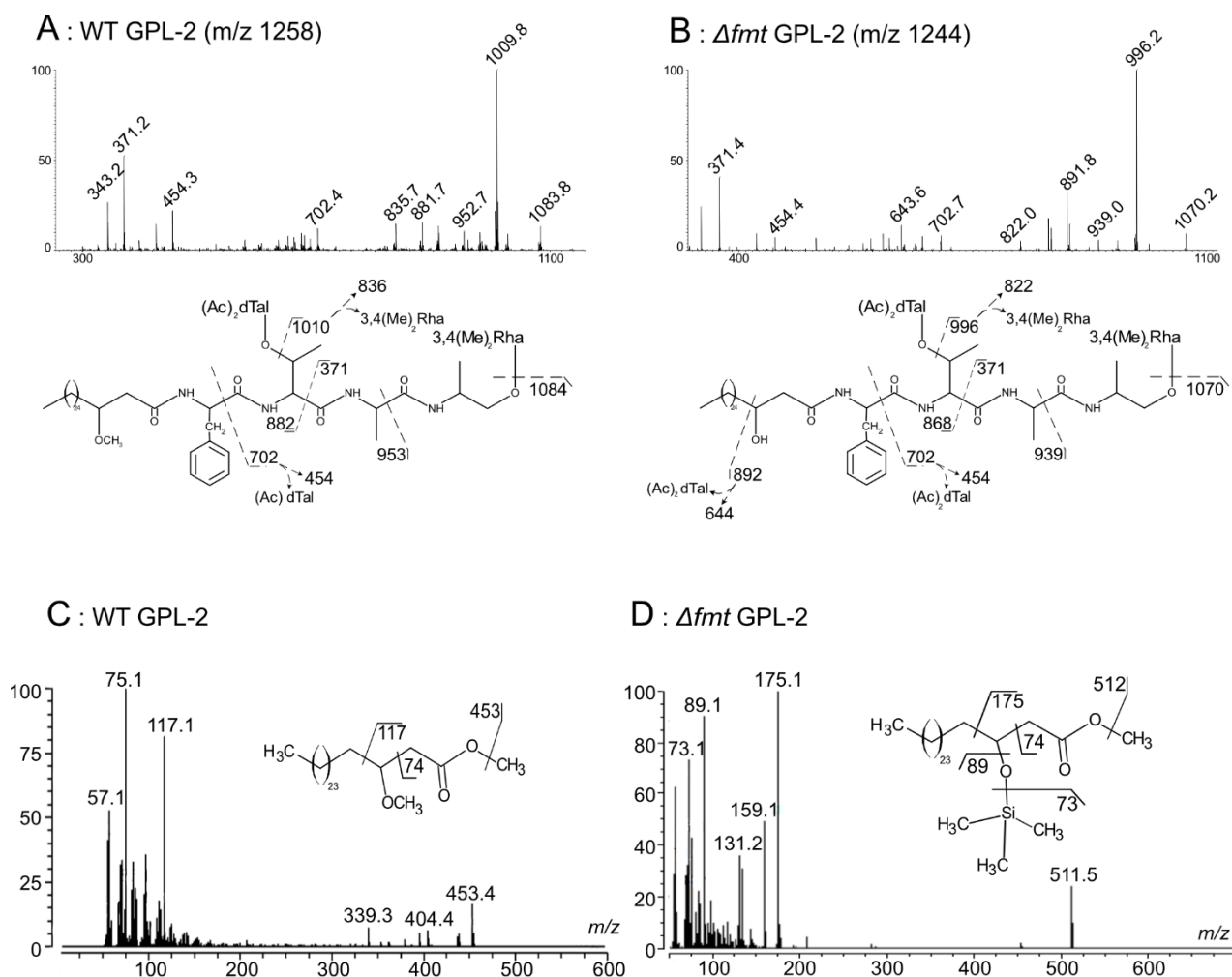
Figure 4. Structural analysis of GPL-2. MS^2 fragmentation spectra of **(A)** the MS signal at *m/z* 1258 of WT GPL-2 and **(B)** at *m/z* 1244 of *Δfmt* GPL-2**.** EI-MS spectra of 3-methoxylated C_{28} FAME isolated from **(C)** WT GPL-2 and its **(D)** 3-trimethylsilylated C_{28} equivalent from *Δfmt* GPL-2.

The fatty acyl chain of GPL lacks a 3-methoxy function in *Δfmt*. NMR was subsequently used to unambiguously identify the origin of the 14 m.u. decrease in *Δfmt* samples. In particular, $^1H/^{13}C$ HSQC heteronuclear experiments confirmed that one signal in the region of O-CH_3 chemical shifts at δ 3.27/57.4 ppm ($^1H/^{13}C$) detected for WT GPL-2 and GPL-3 was absent in the corresponding *Δfmt* fractions **(Figure 3D)**. This signal was clearly identified as a methoxy group associated with the fatty acid chain, according to its chemical shifts reported in *M. smegmatis* [39,40]. In contrast, the two less shielded signals which were similarly observed in all samples were assigned to the O-Me of Me_2Rha, in agreement with previous work [41]. This confirmed that *fmt* has no influence on the methylation of Rha residues. To further certify the loss of methoxylated fatty acids in *Δfmt*, the fatty acid composition of WT GPL and *Δfmt* GPL was investigated by GC/MS. As expected, a mixture of methoxylated fatty acids dominated by a C_{28} octacosanoyl form was identified in WT GPL [40]. Electronic-impact mass spectrometry (EI-MS) fragmentation **(Figure 4C)** of the fatty acid methyl esters (FAME) highlighted the presence of a methoxy group in the 3-position owing to the presence of a specific fragment ion at *m/z* 117. Similar experiments on *Δfmt* GPL did not permit to identify

10

similar methoxylated fatty acids. To identify potential non-methoxylated fatty acids, the free hydroxyl groups of FAME extracted from Δfmt GPL were labelled by trimethylsilylation prior to GC/MS analysis. EI/MS of the reaction products from Δfmt GPL showed the presence of C_{28} octacosanoyl FAME hydroxylated in the 3-position owing to the intense fragment ion at *m/z* 175 **(Figure 4D)**. Finally, exhaustive analysis of MS data of Δfmt GPL-3 revealed that MS^2 spectra of ions at *m/z* 1390 and 1418 generated a specific fragment ion at *m/z* 1038, resulting from the cleavage of the fatty acid C3-C4 bond next to the hydroxyl group that could be further fragmented by MS^3 **(Figure S5A)**. This specific fragment ion was not detected in WT GPL, although an isobaric fragment ion resulting from the cleavage of glycosidic bonds was found by MS^3 analysis **(Figure S5B)**. These data support the view that WT GPL are substituted by 3-methoxylated fatty acids while Δfmt GPL are substituted by their hydroxylated equivalents.

The GXG motif is essential for the methyltransferase activity of Fmt. To investigate whether *fmt* encodes a methyltransferase, the amino acid sequence of Fmt was aligned with other validated methyltransferases using CLUSTALW (https://www.genome.jp/tools-bin/clustalw). The aligned sequences include MT0146/CbiT from *Methanobacterium thermoautotrophicum* [42], the corynebacterial MtrP protein (NCg12764) assisting the transport of trehalose mycolates [43], the methyltransferase catalyzing the transfer of a methyl group onto the lipid moiety of phthiotriol and glycosylated phenolphthiotriol dimycocerosates in *M. tuberculosis* (Rv2952) [44] and the Fmt orthologue in *M. smegmatis* Mtf2 [45], for which active site residues have been identified. In particular, two glycine residues are conserved in *S*-adenosyl methionine (SAM)-dependent methyltransferase and known to be involved in binding to the methyl donor. These correspond to Gly86 and Gly88 in Fmt, which are also conserved in MT0146/CbiT, NCg12764, and Mtf2 **(Figure 5A)**. However, only the second glycine residue is conserved in Rv2952 **(Figure 5A)**. We reasoned that if replacement of these crucial residues by Ala would result in loss of methoxylation, *trans*-complementation of Δfmt with the Ala mutated *fmt* alleles would fail to restore the WT GPL pattern. Thus, Δfmt was transformed with constructs allowing expression of Fmt variants (HA-tagged) in which Gly86 and Gly88 were either individually or simultaneously substituted by Ala. Introducing pMV306-*fmt*-G86A, pMV306-*fmt*-G88A or pMV306-*fmt*-G86A/G88A into Δfmt resulted in similar expression levels of the different Fmt variants, as judged by probing the proteins using anti-HA antibodies **(Figure 5B)**. The TLC profile of the extracted lipids clearly indicates that the introduction of the single or double mutations in *fmt* failed at functionally complementing the GPL profile **(Figure 5C)**.

To support these results, GPL-2 and GPL-3 were purified from Δfmt harboring either pMV306-*fmt*-G86A, pMV306-*fmt*-G88A or pMV306-*fmt*-G86A/G88A and analyzed by MS. As depicted in **Figure S6**, and in agreement with the TLC pattern, the MS profiles in these three strains remain identical to the one in Δfmt. In each of the three Δfmt strains expressing a catalytically-inactivated Fmt variant, GPL-3 fractions displayed a set of intense bands with lower R_f due to a more polar behavior **(Figure S6A)** and identical MS spectra to

Δfmt, with two main ions at *m/z* 1390 and 1418 **(Figure S6C)**. MS[3] analysis of the fragment ion 1418 -> 1038 generated very similar fragmentation pattern to those observed for the *Δfmt* GPL-3 **(Figure S5A)**, strongly suggesting the presence of a β-hydroxyl group on the fatty acid **(Figure S7)**. In addition, the two major ions at *m/z* 1244 and 1272 were found in the GPL-2 fractions of all three strains **(Figure S6B)**. These results establish the absence of methoxylated GPL in *Δfmt* producing the catalytically-inactivated Fmt proteins. Collectively, this indicates that both Gly86 and Gly88 are required for restoring the GPL profile to WT level and confirm that Fmt is a canonical methyltransferase.
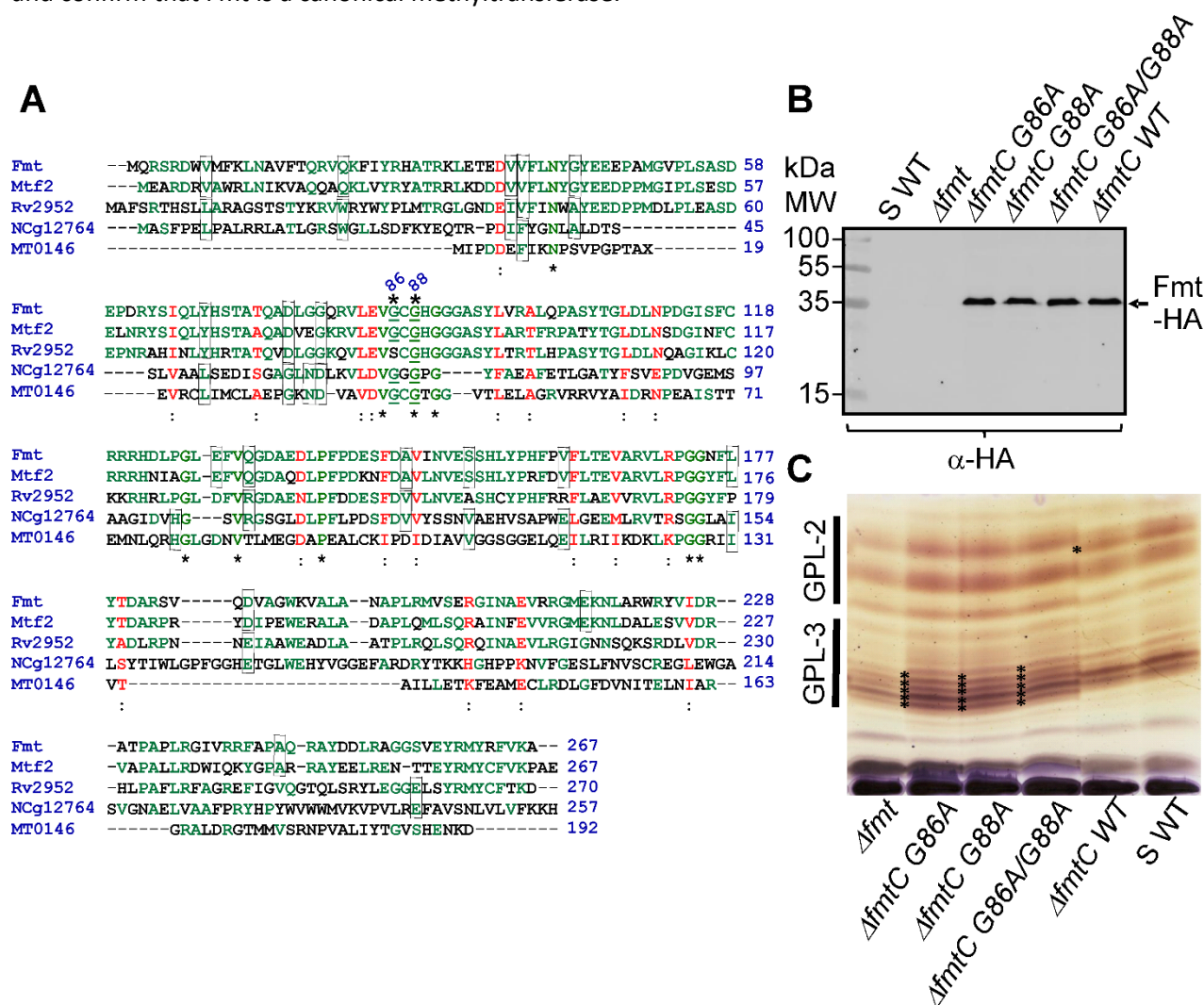
Figure 5. The GXG motif is essential for Fmt activity. (A) Multiple sequence alignment of Fmt with the *Methanobacterium thermoautotrophicum* protein MT0146, the corynebacterial protein NCg12764, the *M. tuberculosis* protein Rv2952 and its orthologue in *M. smegmatis* (Mtf2) using CLUSTALW. Similar residues are shown in red and identical residues are in green. Wherever possible, the two types of identical amino acids were surrounded within the same vertical aligned column. Conserved glycine residues (Gly86 et Gly88) within the GXG motif and mutated in this study are numbered. **(B)** Western blot analysis of the *Δfmt* strain expressing either the Fmt(WT)-HA, Fmt(G86A)-HA, Fmt(G88A)-HA or Fmt(G86A/G88A)-HA fusion proteins under the control of the *fmt* native promotor. **(C)** TLC analysis of the crude lipid fractions of the parental, mutant and the various complemented strains. GPL were separated using CHCl₃/MeOH (9:1, v/v) and revealed after spraying with orcinol and charring. Black asterisks indicate modified GPL species.

Hydrophobicity of *M. abscessus* S is dependent on GPL methylation. Partitioning of mycobacterial cultures between hexadecane and an aqueous buffer has been used as a quantitative marker of hydrophobicity in *M. tuberculosis* evolution and pathogenicity, ranging from the hydrophilic environmental low-pathogenicity ancestors *Mycobacterium kansasii* and *Mycobacterium canettii* to highly hydrophobic virulent tubercle bacilli [46]. To address whether the methylation of GPL affects the surface hydrophobicity of *M. abscessus,* hexadecane-aqueous buffer partitioning was applied to the S, R, *Δfmt* and *ΔfmtC* strains. *M. kansasii* Hauduroy (ATCC 12478) was included as a highly hydrophilic control strain [46]. Consistent with previous findings, the S variant is more hydrophilic than the R variant while *M. smegmatis* mc²155 exhibited an intermediate phenotype [14]. Unexpectedly, *Δfmt*, while producing normal levels of GPL but lacking the methoxy on the fatty acid core, was significantly more hydrophilic than the S variant, almost reaching levels of *M. kansasii,* while complementation restored the wild-type hydrophobic properties of the S strain **(Figure 6A)**. This suggests that lack of *O*-methylation is responsible for the increased hydrophilicity of *Δfmt.*
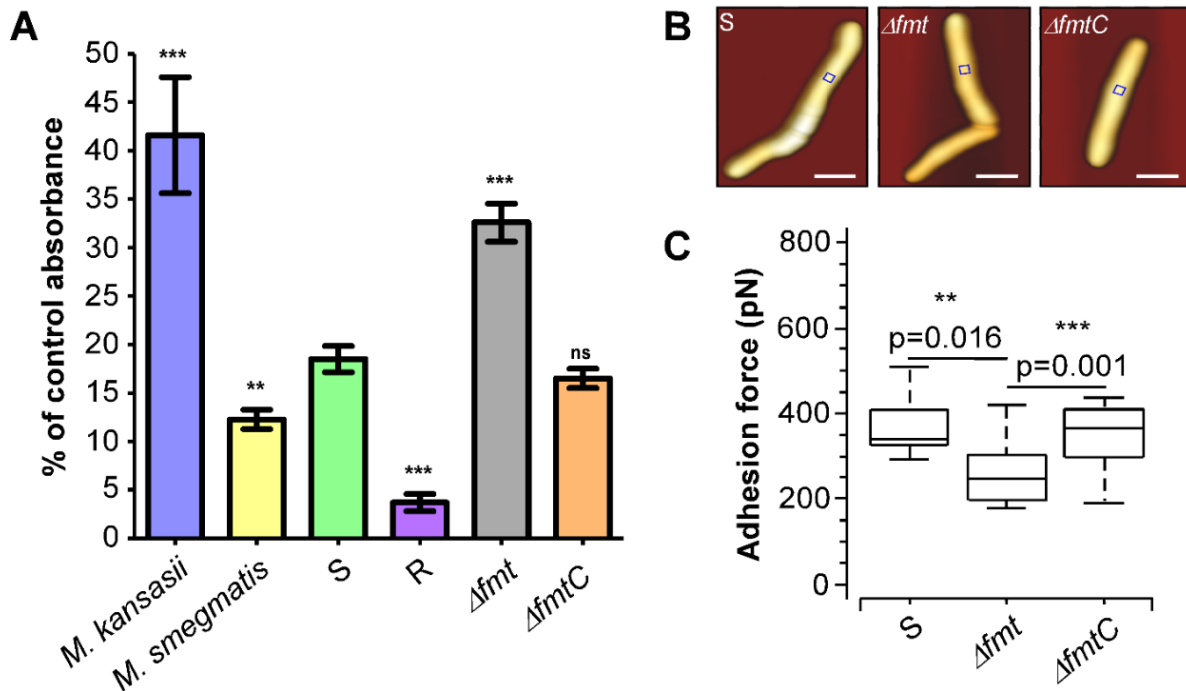

Figure 6. Decreased cell-surface hydrophobicity of *Δfmt*. (A) *M. abscessus* R is more hydrophobic than S, while the *Δfmt* mutant strain's hydrophilicity is significantly higher than S, as assessed by hexadecane partitioning and shown as hydrophobicity index (in percentage of aqueous phase OD prior to partitioning). Histograms and error bars are means ± SD of three independent experiments. Differences between means were analyzed for significance using a two-tailed Student's *t*-test employing Welch's correction for unequal variances. ns, non-significant, [**]$p < 0.01$, [***]$p < 0.001$. **(B)** 3D projections of height images obtained in quantitative imaging (QI) mode of *M. abscessus* S variant wild type (WT), *Δfmt* and *ΔfmtC* cells. The blue squares (250 nm × 250 nm) in each image indicate where adhesion force maps were collected for these representative cells, shown in **Fig. S8** (WT #2, *Δfmt* #5 and *ΔfmtC* #1). Scale bar = 1 μm. **(C)** Boxplots of adhesion forces for *M. abscessus* S wild type (WT), *Δfmt* and *ΔfmtC* cells. Whiskers indicate the range, the bottom and tops of the boxes, the 1st and 3rd quartiles, respectively, and the thick black bar in the middle of the boxes represents the sample median. The different groups were compared using one-way Mann Whitney tests. n = 17 (WT), n = 18 (*Δfmt*), n = 11 (*ΔfmtC*).

Hydrophobic forces are weaker within hydrophobic nanodomains on single *Δfmt* cells. Atomic force microscopy (AFM) with chemically modified (hydrophobic) AFM tips was employed to assay at high spatial resolution the magnitudes, frequencies and surface distributions of hydrophobic adhesive forces on the surface of *Δfmt* [15,47]. Low resolution topographic images (5 μm × 5 μm) were first recorded and then high-resolution adhesion maps were obtained (250 nm × 250 nm, **Figure 6B**, blue squares) on top of the bacteria to avoid edge artefacts. In line with previous work [15], heterogenous distributions of hydrophobic adhesive forces were observed, *i.e.* hydrophobic nanodomains surrounded by hydrophilic areas on the surface of *M. abscessus* S cells **(Figure S8A)** as well as on *Δfmt* **(Figure S8B)** and *ΔfmtC* cells **(Figure S8C)**. The frequencies of detectable hydrophobic forces on *Δfmt* (24 ± 3%, n = 19 cells) did not differ significantly from those on WT bacteria (16 ± 4%) or *ΔfmtC* cells (23 ± 4%), indicating that abrogation of GPL methylation by Fmt does not change the proportion of hydrophobic *versus* hydrophilic areas on the cell surfaces.

To test whether changes in the methylation pattern of GPL affect hydrophobic adhesion within nanodomains, we assessed the average magnitudes of adhesion forces within these domains only (*i.e.* excluding non-adhesive events). The average adhesion force within hydrophobic nanodomains on *Δfmt* was 281 ± 28 pN (mean ± SEM, n = 17, 481 curves from 18 cells), while in WT cells it was 375 ± 37 pN (mean ± SEM, n = 11, 476 curves from 17 cells), a moderate (~25%) but significant difference (*p*=0.016). In *ΔfmtC*, adhesive forces with hydrophobic nanodomains were restored to WT levels (371 ± 20 pN, mean ± SEM, n = 10, 495 curves from 11 cells). These results shown as boxplots in **Figure 6C** indicate that alteration of the GPL methoxylation pattern correlates with changes in the surface hydrophobic properties of *M. abscessus* S cells. It also supports the view that more hydrophobic classes of GPL define the hydrophobic nanodomains exhibited on the surfaces of S variant cells (at least in contribution with other apolar lipid classes). However, that the ratio of hydrophobic to hydrophilic area did not change in *Δfmt* indicates that methoxylation is not the only determinant of GPL hydrophobicity and that other chemical differences between the class of GPL that define the hydrophilic nanodomains and those that define the hydrophobic ones likely exist.

Reduced invasion of THP-1 macrophages by *Δfmt*. Because cell surface hydrophobicity plays important roles such as favoring cell-surface interactions with host tissues [48], the first step leading to infection, we next evaluated the possible impact of GPL methylation on adhesion and invasion of *M. abscessus* by human THP-1 macrophages. Cells were infected with the tdTomato-expressing *M. abscessus* S, *Δfmt* or *ΔfmtC* strains for 3 hrs at a multiplicity of infection (MOI) of 2:1, prior to assessing phagocytosis and rate of replication over time. Following infection, macrophages were treated with 250 μg/mL amikacin for 2 hrs and then amikacin was maintained at 50 μg/mL to prevent extracellular bacterial growth. At 0, 1, 3 and 5 dpi, macrophages were lysed and plated to determine the intracellular bacterial burden. At day 0 (3 hrs post-infection), the invasion rate of *Δfmt* was reduced by almost 50% as compared with the control strain and this effect was rescued with *ΔfmtC* **(Figure 7A)**. This defect was maintained at 1, 3- and 5-days post-

infection **(Figure 7A)**. In parallel, at 0, 1, 3- and 5-days post-infection, macrophages were stained with DAPI and observed under an epifluorescence microscope. Microscopic observations and quantification of the infected cells revealed a pronounced reduction in the number of infected THP-1 cells infected with *Δfmt* just after phagocytosis. Again, this effect was maintained over time as compared to the macrophages infected with either the WT progenitor or *ΔfmtC* strains **(Figures 7B and 7C)**. In contrast, no major effect on bacilli multiplication was observed within the cells, suggesting that *fmt* is important for bacterial invasion rather than for intracellular survival.
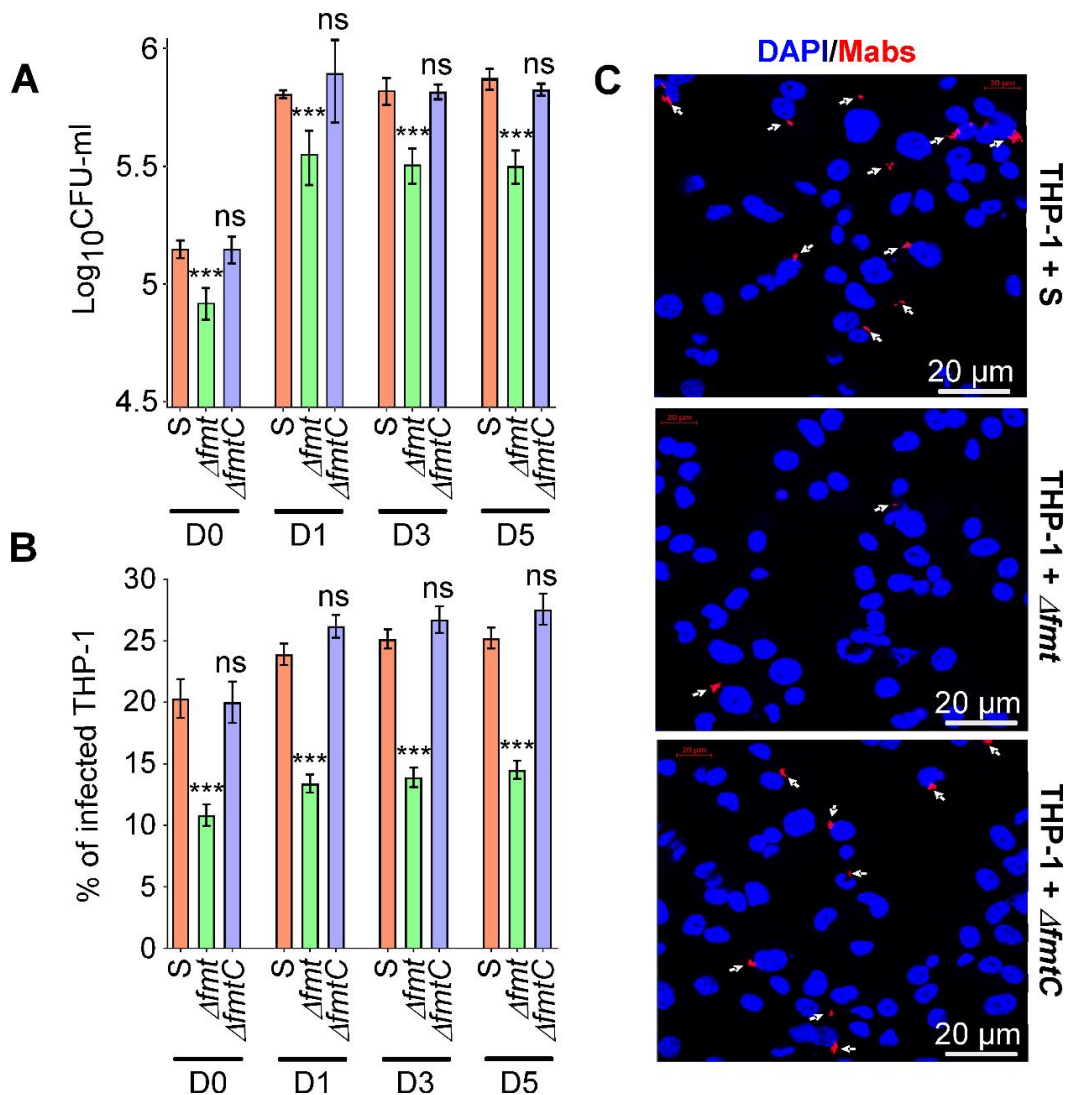
Figure 7. Fmt participates in invasion of human macrophages by *M. abscessus*. Macrophages were infected with the *M. abscessus* S, *Δfmt* and *ΔfmtC* strains expressing tdTomato (MOI of 2:1). **(A)** CFU were determined at days 0, 1, 3 and 5 post-infection. Data are mean values ± SD for three independent experiments. One-tailed Mann Whitney test. ns, non-significant, $^{***}p < 0.001$. **(B)** Percentage of infected THP-1 macrophages at days 0, 1, 3 and 5 post-infection. Data are mean values ± SD for three independent experiments. One-tailed Mann Whitney test. ns, non-significant, $^{***}p < 0.001$. **(C)** Three immuno-fluorescent fields were taken after one-day post-infection at a 40X magnification (using a confocal microscope), showing the nuclei of macrophages infected with the various strains. The nuclei are shown in blue. White arrows indicate mycobacteria within macrophages. Scale bars represent 20 μm. Experiments were done three times independently.

DISCUSSION

This work provides a first glimpse into the structure-function relationship of GPL fatty acid methoxylation. It unambiguously demonstrates that *fmt* encodes a *O*-methyltransferase that catalyzes the transfer of a methyl to the 3-hydroxyl group of the C_{24}-C_{33} fatty acyl chain, with which the amino group of the peptidic core is esterified: i) unmarked deletion of *fmt* leads to the production of GPL carrying a fatty acyl chain lacking a 3-methoxy group while the glycan moiety remains unaltered; ii) substitution of the Gly86 and/or Gly88 residues of the conserved GXG motif, known to bind to the methyl donor in other *O*-methyltransferases [43], resulted in the loss of *O*-methylation of the lipid domain of GPL; iii) Fmt is the orthologue of Mtf2 which methylates GPL in *M. smegmatis* [45]. However, *M. smegmatis* being a non-pathogenic species, the impact of lipid *O*-methylation in the physiopathology of infection cannot be investigated. In addition, we procure strong evidence that *O*-methylation of the GPL fatty acid increases cell surface hydrophobicity of *M. abscessus* and increases internalization of the bacilli by macrophages. By substituting the endogenous promoter of the *mmpS4-mmpL4a-mmpL4b* locus involved in the transport of GPL with a leaky acetamidase promoter from *M. smegmatis* in *M. abscessus* S, we previously reported a strain producing low-GPL levels with a rough appearance, similar to R strains [14]. This rough low-GPL producing mutant was less hydrophilic than the S variant but more hydrophilic than the R variant, indicating that lowering the production of GPL leads to increased hydrophobicity. Herein, we show that *O*-methylation of the lipid core of GPL represents another way for *M. abscessus* to regulate its surface hydrophobicity properties. However, these alterations in the GPL profile were not associated to changes in the susceptibility to cefoxitin, imipenem, bedaquiline, amikacin or rifabutin (data not shown), indicating that methoxylation of the fatty acyl chain does not contribute to the envelope permeability and drug sensitivity of *M. abscessus*.

Earlier comparative studies between the S and R morphotypes of *M. abscessus* underscored the positive correlation between low GPL production and increased hydrophobicity and virulence in animal models [14]. These features are reminiscent of the role that hydrophobicity has played in *M. tuberculosis* evolution towards greater pathogenicity, where more modern pathogenic strains exhibit a higher proportion of less polar lipids in the outer membrane that corresponds with greater surface hydrophobicity [46]. Importantly, increased hydrophobicity may enhance the capability for aerosol transmission, affecting virulence and pathogenicity [46,49]. Conversely, *M. kansasii,* which is much less pathogenic than *M. tuberculosis* and less virulent than *M. abscessus* in the zebrafish model of infection [50], produces large quantities of hydrophilic lipids and is characterized by mycomembrane lipids that are less apolar than those found in *M. tuberculosis* [46]. Our results indicate that *M. abscessus* S is less hydrophilic than *M. kansasii* but more than the R morphotype. Remarkably, that *Δfmt* is more hydrophilic than the S parental strain, indicates that a simple change in the methoxylation pattern of GPL can lead to pronounced phenotypic changes in surface hydrophobicity. However, keeping in consideration the wide heterogeneity of the

microbial population in planktonic cultures, comprising a mixture of bacteria with various degrees of hydrophilicity, we aimed at imaging and quantifying surface hydrophobicity at the single cell level using AFM. As noticed previously, the *M. abscessus* S cell surface is characterized by hydrophilic nanodomains, the latter being completely absent in R variant cells that express homogenous surface hydrophobicity [15], like in other GPL-defective mycobacteria [47,51,52]. While the homogenous hydrophobicity on the R variant cell surface is easily explained by the exposure of more hydrophobic lipid classes, like mycolic acids, in the absence of GPL, two explanations for the presence of both hydrophobic and hydrophilic nanodomains on S variant cells were posited: i) mycolic acids that are hydrophobic (most likely along with other hydrophobic lipids) define the hydrophobic nanodomains, while GPL, which expose relatively hydrophilic head groups, define the hydrophilic nanodomains; ii) more hydrophobic GPL classes define the hydrophobic nanodomains, while hydrophilic nanodomains are defined by more hydrophilic classes [15]. That the average adhesion force within hydrophobic nanodomains on *Δfmt* was lower than in the parental and *ΔfmtC* strains supports the latter hypothesis. It is possible that more apolar GPL-2 define the hydrophobic nanodomains and that a loss of fatty acid methoxylation leads to decreased hydrophobic adhesive forces measured specifically within hydrophobic nanodomains of *Δfmt*. Ensuing studies may explore the contribution of GPL glycosylation profile on surface hydrophobicity.

The fatty acid core of GPL is thought to interact with other lipids present within the outer leaflet of the outer membrane, implying that the methoxy substituent is likely to be buried within the membrane and, presumably, not exposed on the bacterial surface. One cannot, however, exclude that the overall reduced hydrophobicity of *Δfmt* GPL relies simply on direct consequence of the lack of the methoxy group. It is possible that this methoxy group is important for the GPL to interact with other membrane lipids. The loss of the methyl group in *Δfmt* may, therefore, result in "abnormal" interactions with lipids, favoring the exposition of other polar lipids at the bacterial surface, thus influencing the overall cell surface chemical composition and hydrophobic properties. Interestingly, methoxylation has been ascribed to the phenolglycolipids (PGL) and phthiocerol dimycocerosate (PDIM) in *M. tuberculosis*, two other well-described, complex, virulence lipids [53]. In these lipids, the transfer of a methyl group onto the free hydroxyl group of the lipid domain of PDIM and PGL is catalyzed by the methyltransferase Rv2952 [44], whose gene is found within the PDIM/PGL locus, similarly to how *fmt* is located within the GPL locus. Multisequence alignments indicated an overall conservation between Fmt and Rv2952, albeit the GXG motif is not fully conserved in Rv2952 as the first Gly residue is substituted by a Ser. Based on our findings with GPL, it would be interesting to investigate whether the lack of lipid methoxylation in PDIM and PGL translates into altered biological properties and influences pathogenesis of *M. tuberculosis*.

The outermost layer of *M. abscessus* characterizes the interface between bacilli and their host macrophages. It is now clear that the hydrophobic effect is a factor in adhesion of numerous pathogens [48]. Mycobacterial exposed adhesins are recognized by specific cell surface receptors that allow bacteria to

reach and invade their cellular targets. A few adhesins have been shown to play a role in the interaction between mycobacteria and host cells, but their surface position and their approachability to their cognate receptors remain poorly understood. This work shows that the decreased cell surface hydrophobicity of *Δfmt* correlates with reduced invasion of macrophages by *M. abscessus,* while the intracellular growth rate of the mutant was not altered as compared to the one of the WT progenitor. These findings are consistent with previous studies demonstrating that internalization of *M. smegmatis* by human macrophages is more efficient in a mutant lacking GPL (*mps*-inactivated) than in a control strain producing GPL [29,54]. However, whether the reduced adhesion and internalization of *Δfmt* in macrophages is a direct or indirect effect of the lack of GPL methoxylation deserves future investigations. One possibility could be that GPL are direct ligands of macrophage receptors and that the methoxy of the GPL fatty acid chain participates in the ligand-receptor recognition. Improved adherence to target cells is directly correlated with increased bacterial surface hydrophobicity in Neisseria and Streptococci [55,56]. Methylation has also been found to increase hydrophobicity of the outer surface of the flagellar filament in *Salmonella* and, consequently, enhancing bacterial adhesion and host cell invasion [57]. Additional work is required to understand how bacterial surface hydrophobicity can alter the adhesion strength between bacteria and host cells.

CONCLUSION

This study underscores the contribution of GPL methoxylation in the biological functions of this important class of lipids. Because GPL are present in numerous NTM, these results suggest that the activity of Fmt participates in the surface properties and internalization of other NTM, highlighting possible therapeutic interventions against these opportunistic mycobacterial pathogens. Future studies should enlighten the contribution of the other parts of this complex lipid molecule with respect to their biological functions.

METHODS

Mycobacterial strains, growth conditions and reagents. All bacterial strains are listed in **Table S2.** Rough (R) and smooth (S) variants of *M. abscessus* CIP104536^T were usually grown in Middlebrook 7H9 broth (BD Difco) supplemented with 0.05% Tween 80 and 10% oleic acid, albumin, dextrose, catalase (OADC enrichment; BD Difco) (7H9$^{T/OADC}$) at 37°C in the presence of antibiotics, when required. Electro-competent mycobacteria were transformed using a Bio-Rad Gene pulser (25 μF, 2500 V, 800 ohms). For bacterial selection, media were supplemented either with 1 mg/ml hygromycin for strains carrying pTEC27 (Addgene, plasmid 30182), allowing tdTomato expression or with 250 μg/ml kanamycin when harboring the pMV306 derivatives. On plates, colonies were selected either on Middlebrook 7H10 agar (BD Difco) supplemented with 10% OADC enrichment (7H10^{OADC}) or on LB agar. Antibiotics were purchased from Sigma-Aldrich.

***In vitro* growth, colony morphology assays and sedimentation.** Growth was examined by inoculating the mid-log phase cultures into fresh 7H9 at an OD_{600} of 0.05. Cultures were incubated at 37°C with shaking and OD_{600} was monitored for 150 hrs using a Synergy H1 hybrid reader (BioTek). To evaluate colony morphology, bacteria from a log phase bacterial culture (OD_{600}=1) were resuspended in phosphate buffered saline (PBS) and 2 µl of cell suspension were spotted onto $7H10^{OADC}$ or LB agar. Plates were then incubated for 4-5 days at 37°C and colonies were imaged using a Zeiss microscope equipped with a Zeiss Plan Neo Fluor Z 1×/0.25 FWD objective. Images were acquired with an Axiocam503 monochrome (Zeiss) camera and processed using ZEN 2 (blue edition). For sedimentation experiments, cultures were diluted to an OD_{600} of 1 and 2 ml of culture were transferred to a glass tube. Images were taken after 5 min.

Pellicle assays. Pellicle formation was assessed by inoculating 10 µl of mid-log phase mycobacterial cells (OD_{600}, 0.8–1.0) onto medium consisting of M63 supplemented with 10% of glucose, 1 mM $CaCl_2$ and 1 mM $MgSO_4$ and incubated without agitation at 30°C for 5 days.

Hexadecane partitioning. Exponentially growing bacteria were washed twice in PUM buffer (100 mM K_2HPO_4, 54 mM KH_2PO_4, 30 mM urea, 0.8 mM $MgCl_2$) and suspended to an OD_{600} of 0.7. Aliquots (3 ml) were transferred to glass tubes and hexadecane (2.4 ml) added. After a brief mixing, samples were incubated for 8 min at 37°C and phase separation allowed to occur at 22°C for 15 min. The hydrophobicity index was defined as aqueous phase OD_{600}, expressed as a percentage of that of the bacterial suspension in PUM buffer alone [46].

Construction of *Δfmt*. The suicide vector pUX1-*katG* [37] was used to generate pUX1-*katG-fmt* **(Table S3)**, which was subsequently used to generate an unmarked deletion mutant in the S variant of *M. abscessus.* Briefly, the left and right arms (LA and RA, respectively) were PCR-amplified using genomic DNA, Q5 polymerase (New England Biolabs) as well as primers 1 and 2 (LA) and primers 3 and 4 (RA) **(Table S1)**. The purified LA and RA amplicons were restricted with PacI/MfeI and MfeI/NheI, respectively, and ligated to the PacI-NheI-linearized pUX1-*katG,* yielding pUX1-*katG-fmt,* designed to delete 696 bp (87%) of the *fmt* gene. Electrocompetent *M. abscessus* was transformed with pUX1-*katG-fmt.* The selection of bacteria having undergone the first homologous recombination event was done by visual screening of red fluorescent colonies on $7H10^{OADC}$ supplemented with 250 µg/ml kanamycin. After subculturing the culture overnight in $7H9^{T/OADC}$ in the absence of kanamycin, bacterial suspensions were serially diluted and plated onto $7H10^{OADC}$ with 50 µg/ml isoniazid (INH) to select for INH-resistant, Kan-sensitive and non-fluorescent colonies. The DNA junctions were subsequently PCR-sequenced to confirm the proper *Δfmt* genotype.

Complementation constructs. Plasmids for complementation were generated by PCR amplification of *fmt* in fusion with an HA tag sequence under the control of its endogenous promoter region (175 bp) using genomic DNA and the forward primer 9 (containing a KpnI site) and reverse primer 10 (containing an NcoI site as well as the HA-coding sequence) and subsequent ligation into the integrative vector pMV306 cut with KpnI and NcoI, resulting in pMV306-*fmt*. Mutating the Gly86 or/and Gly88 present in the GXG motif in Fmt in pMV306-*fmt* was achieved by site-directed mutagenesis using the primers listed in **Table S1** and the QuikChangeV Site-Directed Mutagenesis Kit (Agilent), according to manufacturer's instructions, yielding pMV306-*fmt*-G86A, pMV306-*fmt*-G88A and pMV306-*fmt*-G86A/G88A. All constructs were verified by DNA sequencing and introduced into *Δfmt*.

Western blotting. Bacteria were harvested, resuspended in PBS, and disrupted by bead beating using 1-mm diameter glass beads. Protein concentration was assessed using the BCA Protein Assay Reagent kit (Pierce), according to the manufacturer's instructions. Equal amounts of proteins (50 µg) were separated by SDS/PAGE and transferred to a nitrocellulose membrane. For detection of Fmt-HA, Fmt-G86A-HA, Fmt-G88A-HA and Fmt-G86A/G88A-HA, membranes were probed for 1 hr with rat anti-HA (dilution 1:2000; Sigma). The KasA protein, used as an internal loading control, was revealed using rat anti-KasA antibodies (dilution 1:2000) [58]. After washing, membranes were incubated for 45 min with goat anti-rat antibody conjugated to HRP (dilution 1:5000; Abcam). The signal was revealed using the ChemiDoc MP system for imaging and analyzing gels (Bio-Rad laboratories).

AFM tip functionalization, sample preparation, parameters and analysis. Gold OMCL-TR400PB-1 AFM probes (Olympus) were functionalized by immersing them in a 1 mM ethanolic solution of 1-dodecanothiol overnight and used fresh. Bacteria were first cultured in 7H9 broth supplemented with 0.2% (w/v) glucose, 0.2% glycerol and 0.025% tyloxapol. At middle exponential phase (OD$_{600}$~ 1.0), bacteria were pelleted by centrifugation, re-suspended in medium lacking tyloxapol, de-aggregated via passing them 10× through a 26 GA syringe needle and finally passing them through a 5 µm PVDF syringe filter (Merck) resulting in a suspension of single bacterial cells. This suspension was seeded into a 35 mm hydrophobic (untreated) microscopy dish (iBidi) and bacteria were left to adhere to the hydrophobic surface overnight at 30°C. Just prior to AFM measurements, the bacteria were washed several times with deionized water and all AFM experiments were performed in ultrapure deionized water. Topographic images were recorded in quantitative imaging (QI) mode using a JPK NanoWizard 4 AFM, bare MSCT probes (k = 0.02) and the following parameters: an applied force of 250 pN, 25 µm/s approach and retraction speeds, a z-length of 500 nm, a map size of 5 × 5 µm and a resolution of 128 × 128 pixels. Adhesion maps were also recorded in QI mode but using hydrophobic probes (k = 0.02) and the following parameters: 25 µm/s approach and retraction speeds, an applied force of 500 pN, a z-length of 500 nm, a map size of 250 nm × 250 nm and a

resolution of 64 × 64 pixels. Owing to tip-geometry induced artefacts that occur on the steep edges of the cells, care was taken to record adhesion maps right on top of the bacteria (250 nm × 250 nm areas). The spring constants of AFM probes were determined empirically using the method of Hutter and Bechhoefer [59]. At least two different tips were used to collect data for each sample and the AFM experiment was repeated on one occasion. Force-distance curves obtained in QI mode were treated using the JPK Data Processing software (V.6.1.125).

Macrophage infection assays. THP-1 macrophages were grown, infected with the *M. abscessus* S, *Δfmt* and *ΔfmtC* strains and processed as reported earlier [60]. At various time points (0, 1, 3- and 5-days post-infection), macrophages were washed three times with PBS and lysed with 100 µl of 1% Triton X100. Cell lysis was stopped by adding 900 µl PBS and serial dilutions were plated to monitor the intracellular bacterial counts. Colonies were counted after 5 days of incubation at 37°C. Microscopy-based infectivity assays were performed as reported previously [60]. Briefly, THP-1 cells were cultivated on coverslips in 24-well plates at a density of 10^5 cells/well. The following day, cells were infected with tdTomato expressing *M. abscessus* (MOI = 2). At various time points after infection, cells were fixed with 4% paraformaldehyde in PBS for 20 min, stained with 1 µg/ml 4',6-diamidino-2-phenylindole (DAPI) for 5 min, washed, mounted onto microscope slides using Immu-Mount (Calbiochem) and examined using a confocal microscope (63x objective) (Zeiss LSM880). Images were acquired and captured on a Zeiss Axio-imager confocal microscope equipped with a 63x oil objective and a camera and processed using Zeiss Axiovision software. Quantification and scoring of the numbers of bacilli present within macrophages were performed within focus using ImageJ. Equal parameters for the capture and scoring of images were consistently applied to all samples. For each condition, ~1000 infected macrophages were analyzed.

GPL extraction. Bacteria grown on 7H10^{OADC} agar plates without detergent were collected and GPL were extracted from the polar lipid fraction, first with chloroform/methanol/0.3%NaCl (9:10:3, v/v/v) and then by chloroform/methanol/0.3%NaCl (5:10:4, v/v/v). The combined solvent extracts were then mixed for 5 min with chloroform and 0.3%NaCl (1:1, v/v) and centrifuged at 3,000 *g* for 5 min to separate the lower-organic phase from the aqueous phase. The upper aqueous layer was discarded and the lower-organic phase was evaporated under a stream of nitrogen and resuspended in chloroform/methanol (2:1, v/v). Polar lipids were then subjected to TLC analysis using Silica gel 60 F$_{254}$ plates (Merck). GPL were separated using either chloroform/methanol/water (90:10:1, v/v/v) or chloroform/methanol (9:1 or 95:5, v/v) and sprayed with orcinol/sulphuric acid vapor prior to revelation by charring.

Glycolipid purification. 1-TLC. For preparative TLC, 150 µl of glycolipid sample was spotted on a 150 mm band on a 60 µm silica gel plate with a glass back (20 cm x 20 cm) and migrated in a solution of

chloroform/methanol/water (90:10:1, v/v/v). Plate sides were sprayed with orcinol in 20 % sulfuric acid and charred to reveal glycolipids while the plate center was reversibly colored with iodide vapor. **2-Flash chromatography.** Glycolipids extracts were impregnated with silica gel overnight. After an equilibration step, impregnated silica was added on top of a low-pressure silica gel column 15 µm, 4 g (INTERCHIM, France) and a linear gradient started on Puriflash (INTERCHIM, France) from 100 % chloroform to reach 85 % chloroform - 15 % methanol at 20 min. This ratio was maintained for 10 min. 6 ml fractions were collected during the gradient phase and the presence of glycolipids was checked by TLC. Fractions containing GPL were pooled, dried and dissolved in chloroform/methanol (2:1, v/v).

GPL saponification and methanolysis. 10 µl of purified GPL was dried under nitrogen, 200 µl sodium hydroxide 0.1 M in chloroform/methanol (2:1, v/v) was added and heated for 2 hrs at 37°C. After the reaction, 1 ml chloroform and 1 ml water were added. The mixture was vortexed for 1 min then centrifuged for 30 sec. The lower chloroform phase was dried under nitrogen and dissolved in 150 µl chloroform/methanol (2:1, v/v). For methanolysis, 10 µl of purified GPL were dried under nitrogen and desiccated overnight, then 200 µl of methanol/HCl 0.5 N was added and heated for overnight at 100°C. After the reaction, 1 ml chloroform and 1 ml water were added. The mixture was vortexed for 1 min, centrifuged for 30 sec and the lower chloroform phase was dried under nitrogen and dissolved in 250 µl heptane.

Itol-acetate derivatives. For hydrolysis step, 1 µg mesoinositol, 20 µl GPL fraction and 1 ml TFA 3M were mixed then heated 4 hrs at 80°C, dried and desiccated overnight. The reduction step was conducted for 4 hrs at room temperature in 500 µL $NaBH_4$ 10 mg/ml in 2M NH_4. The reaction was stopped with concentrated glacial acetic acid. Samples were dried at 55°C under a nitrogen stream by co-distillation with methanol/acetic acid three times, desiccated overnight and incubated in 500 µl anhydride acetic 4 hrs at 80°C. The reaction products were extracted several times with chloroform/water. The chloroform-rich phase was then filtered, dried and dissolved in 100 µl chloroform. Similar experiments were conducted using Rha or 6-dTal standards (CARBOSYNTH, UK).

MALDI-TOF mass spectrometry. Before spotting 5µl on the MALDI plate with a glass capillary tube, 5 µl of 10 mg/ml dihydroxybenzoïc acid (DHB) in chloroform/methanol (1:2, v/v) were mixed with 5 µl of the sample extract in chloroform/methanol (2:1, v/v). MS and MS^n spectra were acquired on an Axima Resonance (SHIMADZU, Kyoto, Japan) in reflectron mode. For MS^2 experiments, collision energy was tuned from 300 eV to 600 eV. For MS^3, ion selection occurred with standard resolution with the same collision energy.

GC-MS analysis. 1-Itol-acetates. 1 µl of itol-acetate derivatives was injected in splitless mode on a Solgel 1 MS 30 m x 0.25 mm x 0.25 µm capillary column with the following gradient temperature: 120°C to 230°C at 3°C/min, then to 270°C at 10°C/min. Compounds were detected after electronic impact at 70 eV on a HP-7820 gas chromatograph coupled to a 5976 single quad (Agilent Technologies, Santa Clara, US) in full scan mode from 50 Da to 500 Da. **2-FAME and TMS derivatives.** After methanolysis, released FAME were extracted in heptane and analyzed on a TRACE 1300 gas chromatograph coupled to an ISQ single quad (THERMO FISHER SCIENTIFIC, San Jose, US). 1 µl was injected in splitless mode on a SLB-5 MS 30 m x 0.25 mm x 0.25 µm capillary column with the following gradient temperature: 50°C to 140°C at 10°C/min, then to 310°C at 15°C/min. After electronic impact at 70 eV, spectra were acquired simultaneously in selected ion monitoring at 74 and 87 Da, and in full scan mode from 50 Da to 700 Da. Trimethylsilyl-derivatives of FAMES were produced by adding 100 µl BSTFA and 100 µl pyridine. After 2 hrs at room temperature, 300 µl heptane was added and processed using the same conditions as for FAME. A methyl 3-hydroxy octadecanoate (MATREYA, US) was also submitted to TMS derivation to check the fragmentation model.

Nuclear Magnetic Resonance. Flash purified GPL were dried and dissolved in a mixture of $CDCl_3/CD_3OD$ (2:1, v/v) with 0.03 % trimethylsilane (EURISOTOP, France) three times then dissolved in a final volume of 200 µl. The sample was then introduced into a 3 mm glass tube (SHIGEMI, Allison Park, PA, US). A TBI probe was used to observe ^1H and ^{13}C nuclei at 293°K on an AVANCE II system (BRUKER BIOSPIN GmbH, Germany). Impulsion sequences used for homonuclear and heteronuclear experiments were from the manufacturer. After acquisition, phase correction and calibration on trimethylsilane signals were performed for δ ^1H and δ ^{13}C. For HSQC, calibration was adjusted on the methanol signal.

Statistical analyses. Statistical analyses were performed on Prism 5.0 (Graphpad) or in R studio (for AFM experiments) and detailed for each figure legend. *$p<0.05$; **$p<0.01$; ***$p<0.001$.

Author contributions

WD conceived and conducted experiments, analyzed the data and wrote the manuscript. LDL, AV and JK conducted experiments. LDL, AV, YFD, YG and LK analyzed the data and participated in writing the manuscript. LK conceived the idea of the project and wrote the manuscript.

Conflict of interest: The funders had no role in study design, data collection, interpretation, or the decision to submit the work for publication. The authors have no conflict of interest to declare.

SUPPORTING INFORMATION

Table S1. List of primers used in this study.
Table S2. List of bacterial strains used in this study.
Table S3. List of plasmids used in this study.
Figure S1. Monosaccharide analysis of purified diglycosylated GPL.
Figure S2. Monosaccharide analysis of purified triglycosylated GPL
Figure S3. MS/MS sequencing of GPL-3.
Figure S4. MS/MS sequencing of saponified WT GPL-3.
Figure S5. MS^3 investigation of *m/z* 1038 fragment.
Figure S6. Analysis of *Δfmt* strains overproducing Fmt(G86A), Fmt(G88A) or Fmt(G86A/G88A).
Figure S7. MS^3 analysis of the *Δfmt* strain transformed with pMV306-*fmt*-G88A, pMV306-*fmt*-G86A or pMV306-*fmt*-G86A/G88A.
Figure S8. Atomic force microscopy with hydrophobic probes.
This information is available free of charge.

REFERENCES

(1)   Johansen, M. D.; Herrmann, J.-L.; Kremer, L. (2020) Non-Tuberculous Mycobacteria and the Rise of *Mycobacterium abscessus*. *Nat. Rev. Microbiol. 18*, 392-407.

(2)   Brown-Elliott, B. A.; Nash, K. A.; Wallace, R. J. (2012) Antimicrobial Susceptibility Testing, Drug Resistance Mechanisms, and Therapy of Infections with Nontuberculous Mycobacteria. *Clin. Microbiol. Rev. 25*, 545–582.

(3)   Esther, C. R.; Esserman, D. A.; Gilligan, P.; Kerr, A.; Noone, P. G. (2010) Chronic *Mycobacterium abscessus* Infection and Lung Function Decline in Cystic Fibrosis. *J. Cyst. Fibros. 9*, 117–123.

(4)   Sermet-Gaudelus, I.; Le Bourgeois, M.; Pierre-Audigier, C.; Offredo, C.; Guillemot, D.; Halley, S.; Akoua-Koffi, C.; Vincent, V.; Sivadon-Tardy, V.; Ferroni, A.; Berche, P.; Scheinmann, P.; Lenoir, G.; Gaillard, J.-L. (2003) *Mycobacterium abscessus* and Children with Cystic Fibrosis. *Emerging Infect. Dis. 9*, 1587–1591.

(5)   Howard, S. T.; Rhoades, E.; Recht, J.; Pang, X.; Alsup, A.; Kolter, R.; Lyons, C. R.; Byrd, T. F. (2006) Spontaneous Reversion of *Mycobacterium abscessus* from a Smooth to a Rough Morphotype Is Associated with Reduced Expression of Glycopeptidolipid and Reacquisition of an Invasive Phenotype. *Microbiology (Reading, Engl.) 152*, 1581–1590.

(6) Medjahed, H.; Gaillard, J.-L.; Reyrat, J.-M. (2010) *Mycobacterium abscessus*: A New Player in the Mycobacterial Field. *Trends Microbiol. 18*, 117–123.

(7) Gutiérrez, A. V.; Viljoen, A.; Ghigo, E.; Herrmann, J.-L.; Kremer, L. (2018) Glycopeptidolipids, a Double-Edged Sword of the *Mycobacterium abscessus* Complex. *Front. Microbiol. 9*, 1145.

(8) Pawlik, A.; Garnier, G.; Orgeur, M.; Tong, P.; Lohan, A.; Le Chevalier, F.; Sapriel, G.; Roux, A. L.; Conlon, K.; Honoré, N.; Dillies, M. A.; Ma, L.; Bouchier, C.; Coppée, J. Y.; Gaillard, J. L.; Gordon, S. V.; Loftus, B.; Brosch, R.; Herrmann, J. L. (2013) Identification and Characterization of the Genetic Changes Responsible for the Characteristic Smooth-to-Rough Morphotype Alterations of Clinically Persistent *Mycobacterium abscessus*. *Mol. Microbiol. 90*, 612-629.

(9) Catherinot, E.; Roux, A.-L.; Macheras, E.; Hubert, D.; Matmar, M.; Dannhoffer, L.; Chinet, T.; Morand, P.; Poyart, C.; Heym, B.; Rottman, M.; Gaillard, J.-L.; Herrmann, J.-L. (2009) Acute Respiratory Failure Involving an R Variant of *Mycobacterium abscessus*. *J. Clin. Microbiol. 47*, 271–274.

(10) Jönsson, B. E.; Gilljam, M.; Lindblad, A.; Ridell, M.; Wold, A. E.; Welinder-Olsson, C. (2007) Molecular Epidemiology of *Mycobacterium abscessus*, with Focus on Cystic Fibrosis. *J. Clin. Microbiol. 45*, 1497–1504.

(11) Ryan, K.; Byrd, T. F. (2018) *Mycobacterium abscessus*: Shapeshifter of the Mycobacterial World. *Front. Microbiol. 9*, 2642.

(12) Madani, A.; Ridenour, J. N.; Martin, B. P.; Paudel, R. R.; Abdul Basir, A.; Le Moigne, V.; Herrmann, J.-L.; Audebert, S.; Camoin, L.; Kremer, L.; Spilling, C. D.; Canaan, S.; Cavalier, J.-F. (2019) Cyclipostins and Cyclophostin Analogues as Multitarget Inhibitors That Impair Growth of *Mycobacterium abscessus*. *ACS Infect. Dis. 5*, 1597–1608.

(13) Bernut, A.; Viljoen, A.; Dupont, C.; Sapriel, G.; Blaise, M.; Bouchier, C.; Brosch, R.; de Chastellier, C.; Herrmann, J.-L.; Kremer, L. (2016) Insights into the Smooth-to-Rough Transitioning in *Mycobacterium bolletii* Unravels a Functional Tyr Residue Conserved in All Mycobacterial MmpL Family Members. *Mol. Microbiol. 99*, 866–883.

(14) Viljoen, A.; Gutiérrez, Ana Victoria; Dupont, C.; Ghigo, E.; Kremer, L. A. (2018) Simple and Rapid Gene Disruption Strategy in *Mycobacterium abscessus*: On the Design and Application of Glycopeptidolipid Mutants. *Front. Cell. Infect. Microbial. 8*, 69.

(15) Viljoen, A.; Viela, F.; Kremer, L.; Dufrêne, Y. F. (2020) Fast Chemical Force Microscopy Demonstrates That Glycopeptidolipids Define Nanodomains of Varying Hydrophobicity on Mycobacteria. *Nanoscale Horiz. 5*, 944-953.

(16) Bernut, A.; Herrmann, J.-L.; Kissa, K.; Dubremetz, J.-F.; Gaillard, J.-L.; Lutfalla, G.; Kremer, L. (2014) *Mycobacterium abscessus* Cording Prevents Phagocytosis and Promotes Abscess Formation. *Proc. Natl. Acad. Sci. U.S.A. 111*, E943-952.

(17) Roux, A.-L.; Viljoen, A.; Bah, A.; Simeone, R.; Bernut, A.; Laencina, L.; Deramaudt, T.; Rottman, M.; Gaillard, J.-L.; Majlessi, L.; Brosch, R.; Girard-Misguich, F.; Vergne, I.; de Chastellier, C.; Kremer, L.; Herrmann, J.-L. (2016) The Distinct Fate of Smooth and Rough *Mycobacterium abscessus* Variants inside Macrophages. *Open Biol. 6*, 160185.

(18) Whang, J.; Back, Y. W.; Lee, K.-I.; Fujiwara, N.; Paik, S.; Choi, C. H.; Park, J.-K.; Kim, H.-J. (2017) *Mycobacterium abscessus* Glycopeptidolipids Inhibit Macrophage Apoptosis and Bacterial Spreading by Targeting Mitochondrial Cyclophilin D. *Cell Death. Dis. 8*, e3012.

(19) Roux, A.-L.; Ray, A.; Pawlik, A.; Medjahed, H.; Etienne, G.; Rottman, M.; Catherinot, E.; Coppée, J.-Y.; Chaoui, K.; Monsarrat, B.; Toubert, A.; Daffé, M.; Puzo, G.; Gaillard, J.-L.; Brosch, R.; Dulphy, N.; Nigou, J.; Herrmann, J.-L. (2011) Overexpression of Proinflammatory TLR-2-Signalling Lipoproteins in Hypervirulent Mycobacterial Variants. *Cell. Microbiol. 13*, 692–704.

(20) Bernut, A.; Herrmann, J.-L.; Ordway, D.; Kremer, L. (2017) The Diverse Cellular and Animal Models to Decipher the Physiopathological Traits of *Mycobacterium abscessus* Infection. *Front. Cell. Infect. Microbiol. 7*, 100.

(21) Catherinot, E.; Clarissou, J.; Etienne, G.; Ripoll, F.; Emile, J.-F.; Daffé, M.; Perronne, C.; Soudais, C.; Gaillard, J.-L.; Rottman, M. (2007) Hypervirulence of a Rough Variant of the *Mycobacterium abscessus* Type Strain. *Infect. Immun. 75*, 1055–1058.

(22) Bernut, A.; Dupont, C.; Sahuquet, A.; Herrmann, J.-L.; Lutfalla, G.; Kremer, L. (2015) Deciphering and Imaging Pathogenesis and Cording of *Mycobacterium abscessus* in Zebrafish Embryos. *J. Vis. Exp. 103*, e53130.

(23) Jankute, M.; Cox, J. A. G.; Harrison, J.; Besra, G. S. (2015) Assembly of the Mycobacterial Cell Wall. *Annu. Rev. Microbiol. 69*, 405–423.

(24) Brennan, P. J.; Nikaido, H. (1995) The Envelope of Mycobacteria. *Annu. Rev. Biochem. 64*, 29–63.

(25) Schorey, J. S.; Sweet, L. (2008) The Mycobacterial Glycopeptidolipids: Structure, Function, and Their Role in Pathogenesis. *Glycobiology 18*, 832–841.

(26) Ripoll, F.; Deshayes, C.; Pasek, S.; Laval, F.; Beretti, J.-L.; Biet, F.; Risler, J.-L.; Daffé, M.; Etienne, G.; Gaillard, J.-L.; Reyrat, J.-M. (2007) Genomics of Glycopeptidolipid Biosynthesis in *Mycobacterium abscessus* and M. Chelonae. *BMC Genomics 8,* 114.

(27) Burbaud, S.; Laval, F.; Lemassu, A.; Daffé, M.; Guilhot, C.; Chalut, C. (2016) Trehalose Polyphleates Are Produced by a Glycolipid Biosynthetic Pathway Conserved across Phylogenetically Distant Mycobacteria. *Cell. Chem. Biol. 23*, 278–289.

(28) Vats, A.; Singh, A. K.; Mukherjee, R.; Chopra, T.; Ravindran, M. S.; Mohanty, D.; Chatterji, D.; Reyrat, J.-M.; Gokhale, R. S. (2012) Retrobiosynthetic Approach Delineates the Biosynthetic Pathway and the Structure of the Acyl Chain of Mycobacterial Glycopeptidolipids. *J. Biol. Chem. 287*, 30677–30687.

(29) Villeneuve, C.; Etienne, G.; Abadie, V.; Montrozier, H.; Bordier, C.; Laval, F.; Daffe, M.; Maridonneau-Parini, I.; Astarie-Dequeker, C. (2003) Surface-Exposed Glycopeptidolipids of *Mycobacterium smegmatis* Specifically Inhibit the Phagocytosis of Mycobacteria by Human Macrophages. Identification of a Novel Family of Glycopeptidolipids. *J. Biol. Chem. 278*, 51291–51300.

(30) Ojha, A. K.; Varma, S.; Chatterji, D. (2002) Synthesis of an unusual polar glycopeptidolipid in glucose-limited culture of *Mycobacterium smegmatis*. *Microbiology 148*, 3039-3048.

(31) Deshayes, C.; Laval, F.; Montrozier, H.; Daffe, M.; Etienne, G.; Reyrat, J.-M. A. (2005) Glycosyltransferase Involved in Biosynthesis of Triglycosylated Glycopeptidolipids in *Mycobacterium smegmatis*: Impact on Surface Properties. *J. Bacteriol. 187*, 7283–7291.

(32) Wiersma, C.; Belardinelli, J. M.; Avanzi, C.; Angala, S. K.; Everall, I.; Angala, B.; Kendall, E.; Moura, V.; Verma, D.; Benoit, J.; Brown, K.; Jones, V.; Malcom, K.; Strong, M.; Nick, J.; Floto, R. A.; Parkhill, J.; Ordway, D.; Davidson, R.; McNeil, M. R.; Jackson, M. C. (2020) Cell Surface Remodeling of *Mycobacterium abscessus* under Cystic Fibrosis Airway Growth Conditions. *ACS Infect. Dis. 6*, 2143-2154.

(33) Sweet, L.; Zhang, W.; Torres-Fewell, H.; Serianni, A.; Boggess, W.; Schorey, J. (2008) *Mycobacterium avium* Glycopeptidolipids Require Specific Acetylation and Methylation Patterns for Signaling through Toll-like Receptor 2. *J. Biol. Chem. 283*, 33221–33231.

(34) Billman-Jacobe, H.; McConville, M. J.; Haites, R. E.; Kovacevic, S.; Coppel, R. L. (1999) Identification of a Peptide Synthetase Involved in the Biosynthesis of Glycopeptidolipids of *Mycobacterium smegmatis*. *Mol. Microbiol. 33*, 1244–1253.

(35) Sondén, B.; Kocíncová, D.; Deshayes, C.; Euphrasie, D.; Rhayat, L.; Laval, F.; Frehel, C.; Daffé, M.; Etienne, G.; Reyrat, J.-M. (2005) Gap, a Mycobacterial Specific Integral Membrane Protein, Is Required for Glycolipid Transport to the Cell Surface. *Mol. Microbiol. 58*, 426–440.

(36) Jeevarajah, D.; Patterson, J. H.; Taig, E.; Sargeant, T.; McConville, M. J.; Billman-Jacobe, H. (2004) Methylation of GPLs in *Mycobacterium smegmatis* and *Mycobacterium avium*. *J. Bacteriol. 186*, 6792–6799.

(37) Richard, M.; Gutiérrez, A. V.; Viljoen, A.; Rodriguez-Rincon, D.; Roquet-Baneres, F.; Blaise, M.; Everall, I.; Parkhill, J.; Floto, R. A.; Kremer, L. (2019) Mutations in the MAB_2299c TetR Regulator Confer Cross-Resistance to Clofazimine and Bedaquiline in *Mycobacterium abscessus*. *Antimicrob. Agents Chemother. 63*, e01316-18.

(38) Lee, M. H.; Pascopella, L.; Jacobs, W. R.; Hatfull, G. F. (1991) Site-Specific Integration of Mycobacteriophage L5: Integration-Proficient Vectors for *Mycobacterium smegmatis*, *Mycobacterium tuberculosis*, and Bacille Calmette-Guérin. *Proc. Natl. Acad. Sci. U.S.A. 88*, 3111–3115.

(39) Gao, J.; Sampson, N. S. (2014) A GMC Oxidoreductase Homologue Is Required for Acetylation of Glycopeptidolipid in *Mycobacterium smegmatis*. *Biochemistry 53*, 611–613.

(40) Lopez-Marin, L. M.; Gautier, N.; Laneelle, M.-A.; Silve, G.; Daffe, M. (1994) Structures of the Glycopeptidolipid Antigens of *Mycobacterium abscessus* and *Mycobacterium chelonae* and Possible Chemical Basis of the Serological Cross-Reactions in the *Mycobacterium fortuitum* Complex. *Microbiology 140*, 1109–1118.

(41) López Marin, L. M.; Lanéelle, M. A.; Promé, D.; Daffé, M.; Lanéelle, G.; Promé, J. C. (1991) Glycopeptidolipids from *Mycobacterium fortuitum*: A Variant in the Structure of C-Mycoside. *Biochemistry 30*, 10536–10542.

(42) Keller, J. P.; Smith, P. M.; Benach, J.; Christendat, D.; deTitta, G. T.; Hunt, J. F. (2002) The Crystal Structure of MT0146/CbiT Suggests That the Putative Precorrin-8w Decarboxylase Is a Methyltransferase. *Structure 10*, 1475–1487.

(43) Rainczuk, A. K.; Klatt, S.; Yamaryo-Botté, Y.; Brammananth, R.; McConville, M. J.; Coppel, R. L.; Crellin, P. K. MtrP, (2020) A Putative Methyltransferase in *Corynebacteria*, Is Required for Optimal Membrane Transport of Trehalose Mycolates. *J. Biol. Chem. 295*, 6108–6119.

(44) Pérez, E.; Constant, P.; Laval, F.; Lemassu, A.; Lanéelle, M.-A.; Daffé, M.; Guilhot, C. (2004) Molecular Dissection of the Role of Two Methyltransferases in the Biosynthesis of Phenolglycolipids and Phthiocerol Dimycoserosate in the *Mycobacterium tuberculosis* Complex. *J. Biol. Chem. 279*, 42584–42592.

(45) Jeevarajah, D.; Patterson, J. H.; McConville, M. J.; Billman-Jacobe, H. (2002) Modification of Glycopeptidolipids by an *O*-Methyltransferase of *Mycobacterium smegmatis*. *Microbiology (Reading, Engl.) 148*, 3079–3087.

(46) Jankute, M.; Nataraj, V.; Lee, O. Y.-C.; Wu, H. H. T.; Ridell, M.; Garton, N. J.; Barer, M. R.; Minnikin, D. E.; Bhatt, A.; Besra, G. S. (2017) The Role of Hydrophobicity in Tuberculosis Evolution and Pathogenicity. *Sci. Rep. 7*, 1315.

(47) Alsteens, D.; Dague, E.; Rouxhet, P. G.; Baulard, A. R.; Dufrêne, Y. F. (2007) Direct Measurement of Hydrophobic Forces on Cell Surfaces Using AFM. *Langmuir. 23*, 11977–11979.

(48) Doyle, R. J. (2000) Contribution of the Hydrophobic Effect to Microbial Infection. *Microbes Infect. 2*, 391–400.

(49) Minnikin, D. E.; Lee, O. Y.-C.; Wu, H. H. T.; Besra, G. S.; Bhatt, A.; Nataraj, V.; Rothschild, B. M.; Spigelman, M.; Donoghue, H. D. (2015) Ancient Mycobacterial Lipids: Key Reference Biomarkers in Charting the Evolution of Tuberculosis. *Tuberculosis (Edinb)95*, S133-139.

(50) Johansen, M. D.; Kremer, L. (2020) A Zebrafish Model of *Mycobacterium kansasii* Infection Reveals Large Extracellular Cord Formation. *J. Infect. Dis. 222*, 1046-1050.

(51) Alsteens, D.; Verbelen, C.; Dague, E.; Raze, D.; Baulard, A. R.; Dufrêne, Y. F. (2008) Organization of the Mycobacterial Cell Wall: A Nanoscale View. *Pflugers Arch. - Eur. J. Physiol. 456*, 117–125.

(52) Dague, E.; Alsteens, D.; Latgé, J.-P.; Verbelen, C.; Raze, D.; Baulard, A. R.; Dufrêne, Y. F. (2007) Chemical Force Microscopy of Single Live Cells. *Nano. Lett. 7*, 3026–3030.

(53) Arbues, A.; Lugo-Villarino, G.; Neyrolles, O.; Guilhot, C.; Astarie-Dequeker, C. (2014) Playing Hide-and-Seek with Host Macrophages through the Use of Mycobacterial Cell Envelope Phthiocerol Dimycocerosates and Phenolic Glycolipids. *Front. Cell. Infect. Microbiol. 4*, 173.

(54) Etienne, G.; Villeneuve, C.; Billman-Jacobe, H.; Astarie-Dequeker, C.; Dupont, M.-A.; Daffé, M. (2002) The Impact of the Absence of Glycopeptidolipids on the Ultrastructure, Cell Surface and Cell Wall Properties, and Phagocytosis of *Mycobacterium smegmatis*. *Microbiology 148*, 3089–3100.

(55) Bartley, S. N.; Tzeng, Y.-L.; Heel, K.; Lee, C. W.; Mowlaboccus, S.; Seemann, T.; Lu, W.; Lin, Y.-H.; Ryan, C. S.; Peacock, C.; Stephens, D. S.; Davies, J. K.; Kahler, C. M. (2013) Attachment and Invasion of *Neisseria meningitidis* to Host Cells Is Related to Surface Hydrophobicity, Bacterial Cell Size and Capsule. *PLoS ONE 8*, e55798.

(56) Araújo, A. M. M.; Oliveira, I. C. M. de; Mattos, M. C. de; Benchetrit, L. C. (2008) Cell Surface Hydrophobicity and Adherence of a Strain of Group B *Streptococci* during the Post-Antibiotic Effect of Penicillin. *Rev. Inst. Med. Trop. Sao Paulo 50*, 203–207.

(57)   Horstmann, J. A.; Lunelli, M.; Cazzola, H.; Heidemann, J.; Kühne, C.; Steffen, P.; Szefs, S.; Rossi, C.; Lokareddy, R. K.; Wang, C.; Lemaire, L.; Hughes, K. T.; Uetrecht, C.; Schlüter, H.; Grassl, G. A.; Stradal, T. E. B.; Rossez, Y.; Kolbe, M.; Erhardt, M. (2020) Methylation of *Salmonella typhimurium* Flagella Promotes Bacterial Adhesion and Host Cell Invasion. *Nat. Commun. 11*, 2013.

(58)   Viljoen, A.; Blaise, M.; de Chastellier, C.; Kremer, L. (2016) MAB_3551c Encodes the Primary Triacylglycerol Synthase Involved in Lipid Accumulation in *Mycobacterium abscessus*. *Mol. Microbiol. 102*, 611–627.

(59)   Hutter, J. L.; Bechhoefer, J. (1993) Calibration of Atomic-force Microscope Tips. *Review of Scientific Instruments 64*, 1868–1873.

(60)   Raynaud, C.; Daher, W.; Johansen, M.; Roquet-Baneres, F.; Blaise, M.; Onajole, O. K.; Kozikowski, A.; Herrmann, J.-L.; Dziadek, J.; Gobis, K.; Kremer, L. (2020) Active Benzimidazole Derivatives Targeting the MmpL3 Transporter in *Mycobacterium abscessus*. *ACS Infectious Diseases 6*, 324-337.